DEVELOPING A MODEL TO PREDICT THE PROPAGATION OF SULFIDE STRESS CORROSION OF STEEL USED FOR PETROLEUM PIPELINES

M.B.A. Deemantha

198044

Degree of Master of Science

Department of Materials Science and Engineering

University of Moratuwa,

Sri Lanka

March 2021

DEVELOPING A MODEL TO PREDICT THE PROPAGATION OF SULFIDE STRESS CORROSION OF STEEL USED FOR PETROLEUM PIPELINES

M.B.A Deemantha

198044

Thesis/Dissertation submitted in partial fulfillment of the requirements for the degree Master of Science

Department of Materials Science and Engineering

University of Moratuwa,

Sri Lanka

March 2021

DECLARATION

I declare that this is my own work and this thesis does not incorporate without acknowledgement any material previously submitted for a degree or Diploma in any other University or institute of higher learning and to the best of my knowledge and belief it does not contain any material previously published or written by another person except where the acknowledgement is made in the text.

Also, I hereby grant to University of Moratuwa the non-exclusive right to reproduce and distribute my thesis/dissertation, in whole or in part in print, electronic or other medium. I retain the right to use this content in whole or part in future works (such as articles or books).

Signature: UOM Verified Signature Date: 2021.11.09

The above candidate has carried out research for the Master's thesis under my supervision.

Name of the supervisor: Dr. G.I.P. De Silva

Signature of the supervisor: UOM Verified Signature Date 2021.11.09

ABSTRACT

Sulfide stress corrosion (SSC) is a deleterious type of corrosion that is abundant in petroleum refineries. SSC easily attacks oil country tubular goods (OCTG) in petroleum refineries. The main factors that affect SSC can be identified as the pressure/tensile stress applied on the metal, H_2S concentration and time period. It can be identified that the environmental conditions of petroleum refineries provide optimum conditions for the initiation and propagation of SSC. Therefore petroleum refinery plants conduct time-basis routine inspections to detect the sulfide stress corrosion. When a severe corrosion is detected at an inspection routine, pipelines are required to be replaced. The unusual behavior of the propagation of SSC cracks may lead drastic failures before it is identified through an inspection routine. Therefore the petroleum industry is expecting to use an accurate model that can predict the initiation and propagation of sulfide stress corrosion. However, the mechanism of SSC has not been clearly revealed yet.

The principle aim of this study is developing a model that can predict the propagation of depth of sulfide stress corrosion in API 5L Grade B steel as a function of applied load (tensile load), pH value and time duration. API 5L Grade B steel was procured from Sri Lanka petroleum corporation as a seamless pipe. The model has been established based on the experimental values of depth of sulfide stress corrosion under different predetermined test environmental conditions kept within the pH value of 2.7 – 3.5, applied load of 400 – 800 N and time duration of 15 – 45 days. The depth of sulfide stress corrosion was measured using the scanning electron microscope images of cross sections of corroded steel specimens. The temperature and the pressure of the test environments were maintained at 24±3 ^{0}C and 1 atm respectively. Further, the model was validated by another data set obtained within the aforementioned, same ranges of parameters. All the laboratory experiments were conducted in accordance with ANSI/NACE TM0177-2016 standard test method.

In addition to the development of the model, the propagation behavior of SSC was investigated under the above mentioned different test environmental conditions. The microstructures that were observed through scanning electron microscope (SEM) and

SEM/EDAX elemental profile plots were obtained to investigate the Sulfur distribution within the crack.

According to the experimental results, it was able to develop a model that predicts the propagation of depth of sulfide stress corrosion. The model prediction values were in good agreement with the experimental values. However model tends to underestimate the depth of corrosion values when time duration closes to 30 days. Since the model has been constructed and validated within the pH value from 2.7 to 3.5, applied loads from 400 N – 800 N and time durations from 15 days to 45 days, the model is expected to be given the accurate predictions only within the aforementioned test environmental conditions.

The SEM images of cross sections of corroded specimens showed that crack initiation occurred after 15 days at all different test environmental conditions. Further, crack propagation occurred transversely, developing branches through the cross section until 30 days of time duration and the behavior of the propagation of crack was completely changed at 45 days of time duration.

ACKNOWLEDGEMENT

This work is not achieved only by myself, but it is an achievement I had through supports of numerous individuals. First and foremost I would like to express my deepest gratitude to my supervisor Dr. G.I.P. De Silva. He provided me with a great opportunity to join with this research project and has always been supportive to accomplish my objectives. His unstinting guidance and constructive feedback improved my research ability and professional skills.

I would like to thank Prof M. Narayana and Dr. (Mrs.) N.M.V.K. Liyanage for their immense support and academic push throughout the evaluation procedure. Next, I would like to thank Ceylon Petroleum Corporation for providing steel samples for research works.

Further, I would like to thank all academic and nonacademic staff of department of materials science and engineering, University of Moratuwa for supporting me to conduct my research works in a better academic environment. Lastly, I convey my love and gratitude to my parents for their constant support.

TABLE OF CONTENTS

LIST OF FIGURES

LIST OF TABLES

DEVELOPING A MODEL TO PREDICT THE PROPAGATION OF SULFIDE STRESS CORROSION USED IN PETROLIUM PIPELNES

1 INTRODUCTION

1.1 Research background and problem statement

Sulfide stress corrosion (SSC) is a type of hydrogen embrittlement (HE) or stress corrosion cracking that occurs due to the synergistic effect of tensile stress and corrosive environment including H_2S. SSC can easily be found in steel when the steel is in an environment where it finds the aforementioned conditions that require occurring the corrosion. These environments are called sour environments and hence this corrosion is called as sour corrosion as well.

The petroleum industry is one of the main industries which emit H_2S gas to the environment. Therefore petroleum refineries are rich with H_2S, either in dry condition or in wet condition. Sulfide stress corrosion occurs when H_2S is in wet condition. The concentration of H_2S is a major factor of the behavior of sulfide stress corrosion. In addition to the H_2S concentration (pH value), it has been found that the applied stress (applied load), time duration, iron sulfide scale, temperature, flow effects, solution composition and other chemicals such as, inhibitors, glycol, biocides, demulsifiesetc. effect the behavior of sulfide stress corrosion[1]. But most of the literatures mention that the effects of these parameters are confusing [2]. However pH value, time duration and applied stress (applied load or pressure) are considered as the most effecting factors on the behavior of sulfide stress corrosion [1][3]. It has been found that the iron sulfide (FeS) scale which is produced as the corrosion product is also effects the behavior of the propagation of sour corrosion. The types of iron sulfide scales that can be formed due to the sour corrosion are amorphous iron sulfide, Mackinawite, pyrrhotite, cubic iron sulfide, troilite, marcasite, pyrite, etc [1]. But experiments have proven that the most

abundant iron sulfide species is Mackinawite in sour corrosion product [4]. Therefore Mackinawite is the main polymorph of iron sulfide which effects the behavior of the propagation of sulfide stress corrosion. Further, it can be concluded that the whole mechanism of the propagation of sulfide stress corrosion depends on the chemical and physical properties of Mackinawite [4].

Although flow effect is mentioned as an effecting factor, most of the literatures evidences that it has very little effect on sour corrosion [1][5][6]. Some literatures mention that it effects only at the very beginning of a considered sour corrosion process.

Temperature is also an important factor but depending on the temperature, the sour corrosion may be either sulfide stress cracking or stress corrosion cracking. With the presence of tensile force and sour conditions, Sulfides stress cracking is predominant under low temperature (-10 ^{0}C to 50 ^{0}C) while the stress corrosion cracking is predominant under higher temperatures (above 50 ^{0}C) [3][7].

Since petroleum refineries are rich with aforementioned factors, sulfide stress corrosion has become a critical problem that requires immediate and permanent solutions in petroleum industry. The best way to avoid sulfide stress corrosion is removing the factors that affect sulfide stress corrosion. But it is impossible due to the sour environment which presence in the petroleum industry. During the past fifteen years, the petroleum industry focused on the production of natural gas from deep wells (Sour wells). It is obvious that the pressure inside these deep wells gets a comparatively higher value. Sometimes, the value of the formation pressure of natural gases exceeds 140 MPa. This high pressure inside sour wells make a likelihood for the contamination of hydrogen sulfide with natural gases. [8].

Selecting sulfide stress corrosion resistive materials to manufacture oil country tubular goods (OCTG) is an acceptable solution. Generally alloy steels of chromium, nickel, manganese and niobium are SCC resistive materials and can be used to manufacture OCTG to get rid of SCC. But still the industry is using low carbon or medium carbon steels to manufacture OCTG as the aforementioned SCC resistive alloys are not cost

effective. Therefore mitigation of SCC has become little difficult in the petroleum industry.

Instead of preventing SSC, identifying SSC at early stage is a practical approach to avoid the adverse effects of SSC. Number of failures and number of accidents occur due to sulfide stress corrosion in petroleum industry since SSC propagates without giving a prior warning [9]. Hence, if it is possible to identify the development of SSC using a model, it would be more advantageous and practical. The existing techniques which are used to track the sulfide stress corrosion are not considerably predict the behavior of SSC. They indicate the extent that the corrosion has propagated. The existing techniques such as nondestructive testing, scanning electron microscope image analysis, optical techniques and electro chemical techniques [10] cannot be used to predict the propagation of sulfide stress corrosion. These techniques are used in time basis inspection routines and these inspection routines do not reveal corrosion propagation rate or any other information that helps to estimate the time duration that the failure may occur.

Prediction models have been developed over the past fifteen years to predict the sulfide stress corrosion but most of them have failed to predict the corrosion rate or corrosion behavior accurately. The rest of the models are predicting the accurate results under certain conditions. Some of the models tend to predict wrong results when they are predicting corrosion behavior at higher time durations [11]. Some of the models predict accurate results when they are predicting corrosion behavior at very low H_2S concentrations [12]while some models predict accurate results at high H_2S Concentrations [11][13].

Since an accurate model has not been developed till now, researching on developing a SSC prediction model has become an essential title in corrosion researches. The main reason of predicting wrong results by developed models can be identified as the complex mechanism of corrosion propagation which has not been found yet. Although it is said that SSC is propagated due to the formation of FeS by direct heterogeneous reactions

happens between Fe^{2+} and S^{2-}, none of the researcher could explain the full mechanism of propagation of SSC.

The researches that have been carried out up to date has been conducted for different materials and different test conditions. The test conditions for each research had been selected depending on the field conditions that the research was focusing. Similarly the materials had also been selected based on the materials which had been used to manufacture respective OCTG. Some of the common materials that have been subjected by sulfide stress corrosion cracking experiments are API 5L grade B steel, AISI 4137H steel, AISI 1018 carbon steel, 20# steel, X65 pipeline steel, FV520B steel etc [14][15]. It can be seen that metals used in OCTG are mainly steel types [3].

Sri Lanka Petroleum Corporation is using pipelines which are made out of API 5L grade B Steel. Petroleum Corporation is responsible for the refining of imported crude oil and distributing refined products all over the island.

1.2 Objectives

1. To study the correlation of applied load, H_2S concentration and time period with corresponding depth of corrosion.
2. To develop a model to predict the depth of corrosion occurred under different H_2S concentrations, loads and time periods.

2 LITERATURE SURVEY

2.1 Mechanisms of SSC cracks propagation

Different models have been developed to predict the behavior of sulfide stress corrosion over past 15 years. These models have proposed different mechanisms for the propagation of sulfide stress corrosion. It can be seen that these models have been developed focusing either the sulfide stress cracking or H_2S corrosion due to direct heterogeneous reactions. Generally these types of corrosions are known as sour corrosions. Some of the models are pure empirical models, some are semi empirical models and some models are pure theoretical models.

Most of the models have been developed assuming the phenomenon of hydrogen embrittlement or diffusion controlled hydrogen permeation. But some models have assumed that sulfide stress corrosion happens due to direct heterogeneous reactions which occur between Fe^{2+} and S^{2-}[11]. Some models predict the corrosion in terms of electrochemical nature of reactions which occur at the propagation of sulfide stress corrosion [13]. Modeling of sour corrosion, assuming diffusion phenomenon is another method of prediction of sour corrosion [12]. Nature of the propagation of mechanical ruptures in the corrosion product is another concept used at modeling of this corrosion type [14].

At empirical modeling, propagation of sulfide stress corrosion have been defined based on the crack propagation, crack formation, depth of the crack, force required to failure and cohesive stress at crack tip etc. [12][13][14].Theoretical models have used mechano-chemical theories, electro-chemical theories, and numerical methods etc. Furthermore, models have used slip dislocation theories, fracture mechanics, reaction kinetics etc. [11][15][16].

Based on the details, available models have been developed based on different criterion of crack propagation [8]. Some of the criteria are shown below.

1. Configuration of cracks: cracks which are stationary or growing, cracks which are developed at the surface or in the bulk of metal, cracks developed due to external loads or internal pressure build up.
2. Origin of hydrogen: Hydrogen are supplied internally through the metal or externally through environment, hydrogen are supplied from the crack surface or away from the surface.
3. Diffusion phenomena of hydrogen: Concentration driven diffusion or/and stress driven diffusion, fragile or solid couplings associated with crack tip formation transient diffusion or steady state diffusion, microstructure based traps or plastic strain based traps, unidimensional or multi-dimensional diffusion, explicit studies of trapping approximation or analytical approximation.
4. Crack tip mechanics: leaner elastic fracture mechanics or elastoplastic fracture mechanics, explicit analysis of stress or moderated analytical solution, small deformation or finite deformation theory, fragile or solid coupling in the localized H concentrations, conventional plasticity and non-conventional plasticity.
5. Failure criterion: Hydrogen pressure based failure, decohesion based failure, plasticity based failure.
6. Criterion for the propagation of crack depth: Diffusion phenomena, cracks propagations due to mechanical stresses, direct heterogeneous reactions.

As mentioned earlier, hydrogen embrittlement is one of the main phenomena that considers at propagation of sulfide stress corrosion. There can be identified four main mechanisms for hydrogen embrittlement [16]. They are stress induced hydride formation, hydrogen enhanced localized plasticity, hydrogen enhanced decohesion and hydrogen pressure theory.

Hydrogen pressure theory states the crack propagation occur due to the pressure which is grown at sharp crack tip. The pressure developed at the end point of crack is increased when concentration of H_2 in voids, grain boundaries or interstitials get increased. This mechanism can be used to describe the sudden failure phenomena associated with

sulfide stress cracks [17]. Some experiments reveal that high pressures were detected at voids (internal voids, interstitials or grain boundaries) even if the partial pressure of hydrogen is very low [18]. This imply that hydrogen pressure theory cannot be used isolated to describe the SSC propagation phenomena.

Hydrogen enhanced decohesion theory states inter atomic bonding gets weaken with the hydrogen diffusion into precipitates, interstitials and grain boundaries. The bonds are broken when the hydrogen diffusion increased to accommodate slip [19]. This mechanism can be used to explain the load relaxation during the tensile test and intergranular failure [8].

Hydrogen enhanced localized plasticity was introduced by Beachem in 1972 as a new concept for hydrogen assisted cracking. In 1994 he explained that hydrogen enhanced localized plasticity happens with reduction of barriers for the dislocation motion, thereby populating the deformation in higher amount adjacent to the fracture surface in a localized region [20]. This starts to happen when H in a solid solution increased. Metal microstructure, crack tip stress intensity and concentration of hydrogen are the main factors that affect the hydrogen enhanced localized plasticity. More precisely, Beachem's model suggests that dislocations are multiplied with the effect of hydrogen and move inside the steel under decreased stress values. Further it says that dislocation motion is not locked by the effect of hydrogen. If these hydrogen atoms are adsorbed at the crack tip or at the voids, adsorption induced dislocation emission mechanism may occur. This is also a mechanism of hydrogen embrittlement that may leads sulfide stress corrosion when suitable environmental conditions take place [8].

There is another hydrogen embrittlement called stress induced hydride formation. But this hydrogen embrittlement mechanism cannot be used to describe sulfide stress corrosion in steel. The reason is that stress induced hydride formation doesn't concern iron and nickel alloy. But titanium, zirconium and vanadium are subjected severely to hydrogen embrittlement. Even at low hydrogen concentration, below the solid solubility limit, stress-assisted hydride formation enhance embrittlement, which is enhanced by

slow straining. At higher hydrogen concentrations above the solubility limit, brittle hydrides are precipitated on slip planes and cause severe embrittlement.

In addition to the hydrogen embrittlement phenomena, diffusion phenomena and mechanical ruptures occurs due to mechanical stresses in corrosion product have been used to describe the propagation of sulfide stress cracks. The formation of initial uniform FeS layer due to the heterogeneous reactions[12] have been described using simple equilibrium reactions as mentioned below[11][21].

Dissolution of H_2S

$$H_2S_{(g)} \longleftrightarrow H_2S_{(aq)} \quad \text{.....(a)}$$

Dissociation of H_2S

$$H_2S_{(aq)} \longleftrightarrow HS^-_{(aq)} + H^+_{(aq)} \quad \text{.....(b)}$$

Dissociation of HS^-

$$HS^-_{(aq)} \longleftrightarrow H^+_{(aq)} + S^{2-}_{(aq)} \quad \text{..... (c)}$$

Reduction of H_2S

$$2H_2S_{(aq)} + 2e^- \longleftrightarrow H_{2\,(g)} + 2HS^-_{(aq)} \quad \text{.....(d)}$$

Dissolution of Fe

$$Fe_{(s)} \longleftrightarrow Fe^{2+} + 2e \quad \text{.....(e)}$$

Formation of FeS by the mechanism of precipitation

$$Fe^{2+}_{(s)} + S^{2-}_{(aq)} \longleftrightarrow FeS_{(s)} \quad \text{.....(f)}$$

Final corrosion product is FeS where FeS exists as Mackinawite which is one of the polymorphs of FeS [12]. The initial FeS layer formation has been considered by some experiments similar to general corrosion of H_2S [11] [12]. Experiments suggests that the whole corrosion process is led by diffusion phenomenon that has been mainly categorized as convective diffusion, molecular diffusion and solid state diffusion.

The following equations of each diffusion type have been taken into account to develop models.

The equation for the Convective diffusion,

$$Flux_{H2S} = K_{m,H2S}\,(C_{b,H2S} - C_{O,H2S}) \ldots 1$$

The equation for the Molecular diffusion,

$$Flux_{H2S} = \frac{D_{H2S}\varepsilon\varphi}{\delta_{OS}}(C_{O,H2S} - C_{i,H2S}) \ldots..2$$

The equation for the solid state diffusion,

$$Flux_{H2S} = A_{H2S}e^{\frac{-B_{H2S}}{RTk}}\ln(\frac{C_{i,H2S}}{C_{s,H2S}}) \ldots\ldots\ldots 3$$

Note that the interfaces for the convective, molecular and solid state diffusion are mass transfer boundary layer, liquid in the porous outer scale of Mackinawite and inner Mackinawite film.

Where,

$Flux_{H2S}$ is stated in mol/ (m^2s)

$K_{m, H2S}$ - coefficient of mass transfer for H_2S in the hydrodynamic boundary layer, $k_{m, H2S}$ = 1.00 ×10^{-4} in approximately static conditions, in m/s.

$C_{b, H2S}$ - bulk concentration of H_2S in the liquid phase in mol/m^3.

$C_{O, H2S}$ - interfacial concentration of H_2S at the outer scale/ solution interface in mol/m^3

$D_{H2S}$is the diffusion coefficient for dissolved H_2S in water, D_{H2S} = 2.00 × 10^{-9}, in m^2/s

E is the outer Mackinawite scale porosity.

Φ - Outer Mackinawite scale tortuosity factor.

$C_{i, H2S}$ - interfacial concentration of H_2S at the inner scale/ film interface in mol/m^3

δ_{os} - thickness of the Mackinawite scale, $\delta_{os} = m_{os} / (\rho_{FeS} A)$ in meter.

m_{os} - mass of the Mackinawite scale in kg

ρ_{FeS} - density of Mackinawite

A - Surface area of the steel in m^2.

A_{H2S}, B_{H2S} – Arrhenius constants, A_{H2S} = 1.30 × 10^{-4} mol/m^2s and B_{H2S} = 15500 j/mol

T_k - Temperature in Kelvin

$C_{s,\ H2S}$ - Concentration of H_2S on the steel surface and when it is set to 1.00×10^{-7} in mol/m^3.

Once the Mackinawite layer is formed, the mechanical stress on Mackinawite causes to make multiple ruptures at different places. Researches reveal that sulfide stress cracks are formed due to these ruptures.

Once the initial corrosion product (Mackinawite) is formed, cracks start to propagate while the corrosion process continues. Propagation of corrosion and cracks can be described using the concept of mass transfer with the aids of the structure of Mackinawite. This is another popular concept of the mechanism of propagation of sulfide stress cracking that the researchers use to explain. The structure of Mackinawite is described according to the literatures below.

2.2 Mackinawite

Mackinawite forms on steel surfaces when FeS is soluble in bulk solution. That means Mackinawite forms when FeS is below the bulk solution saturation limit and H_2S is equal or greater than the level required for Mackinawite formation [14]. If these conditions are violated, another types of FeS such as pyrrhotite, pyrite, marcasite, troilite, greigite, smythite or Cubic FeS may form. Contrary, some of the researchers explain when a clean surface of metal is exposed to a sour environment (H_2S rich environment), Mackinawite starts to form if the formation of FeS is thermodynamically stable. Further, they elaborate this formation of Mackinawite occur even at very small concentrations of H_2S. [4].

Since petroleum sour environments are friendly to Mackinawite formation environmental conditions, majority of sulfide stress cracking based experiments have been conducted assuming the corrosion product is Mackinawite.

Mackinawite is a nonstoichiometric, iron excess form of FeS. The mineral is designated as $Fe_{1+x}S$. However, Rickard [22] proved through his experiments that Mackinawite is stoichiometric. He mentioned that the wrong assumption had been made due to some

issues involved in analytical procedures at analyzing Mackinawite. The main problem associated with the analytical procedure was the loss of little amount of sulfide when Mackinawite is dissolved. This made a minuscule change in the stoichiometric ratio.
This made an assumption such that the Mackinawite is not a stoichiometric compound. Later, the analytical method was changed such that it avoided the loss of elemental sulfur and he proved that the Mackinawite is stoichiometric. Mackinawite can be detected using X – ray diffraction technique and it is the only analytical technique that can be used to detect Mackinawite over the other types of FeS [14]. Mackinawite has a layered or sheet like structure as shown by Figure 2.1. When the structure is explained in terms of crystallography, it can be seen that the distances of inter-atomic bonds between iron atoms gets a higher value compared to the distances of inter-atomic bonds between iron and the other atoms (oxygen) in the Mackinawite. So it makes thin sheets which are basically separated by Fe atoms (Figure 2.1) [23]. These so called sheets are grown on a ferritic surface. Figure 2.2 illustrates how Mackinawite structure is placed on the ferritic surface.

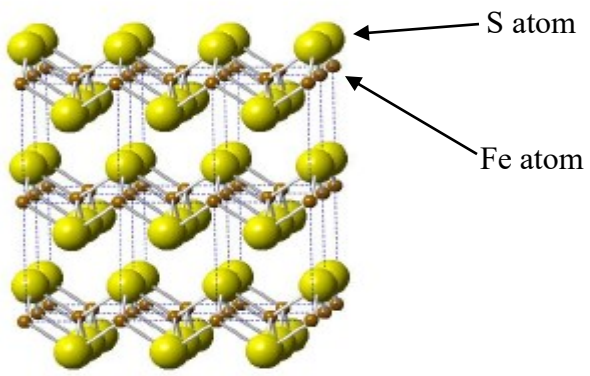

Figure 2.1 : Crystal structure of Mackinawite [23]

This crystal structure provides enough evidence to prove that Mackinawite is a good electrical conductor [24]. Therefore, a good electrical conductivity can be expected from Mackinawite surface to the ferritic iron surface across the Mackinawite layer. However, the electrical conductivity is believed to be performed well along the planar orientation of the precipitation than it performs along the normal direction to the planes.

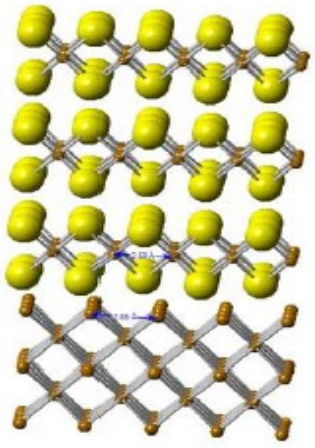

Figure 2.2: Growth of Mackinawite on the foundation of ferritic surface [23]

Further, the electrical conductivity of Mackinawite is greater compared to the electrical conductivities of other types of FeS [4] [24].

In addition to the electrical conductivity, this planer structure of Mackinawite provides a significant property which causes the propagation of corrosion of the metal where the Mackinawite is placed on. Zhao and liu[25] explains that Mackinawite can adsorb divalent metallic cation in to the lattice. Once these cations are adsorbed by Mackinawite, they can intercalate between the sheets of Mackinawite as shown in Figure 2. 3. This is an interesting as well as significant property in sulfide stress corrosion.

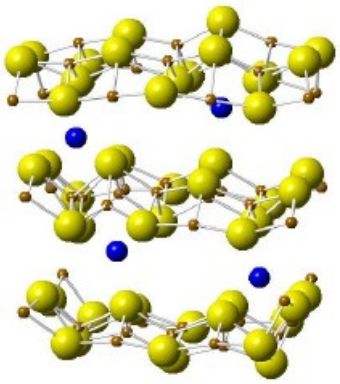

Figure 2.3: Movement of cations through Mackinawite layers [23]

2.3 Propagation of sulfide stress crack

Once the Mackinawite layer forms through direct heterogeneous reactions as shown in equation 6, the thickness of the Mackinawite layer begins to increase its thickness still the bulk solution has access to metal surface and the dissolution rate is less than the growth rate.

The dissolution rate of Mackinawite depends upon environmental conditions such as dissolved H_2S Concentration, Surface pH and temperature. However, if the bulk solution is continuously replenished, Fe^{2+}ion concentration remains low causing continuous dissolution of Mackinawite. This leads continuous degradation of metal surface. But if the corrosion happens in a constant volume chamber, Fe^{2+} concentration is increased by the dissolution of Mackinawite with time. Hence dissolution reaction gets slow down increasing the growth of Mackinawite layer. In real conditions, low concentrations of Fe^{2+} are maintained only at new fields. However, the older fields get higher concentrations of Fe^{2+}in the solution which passes through the pipelines [4].

With the initiation of the Mackinawite layer, rapid growth of corrosion layer begins. Sun [12] explains this continuous growth of corrosion layer is interrupted with the formation of ruptures which are originated by the mechanical stresses developed at Mackinawite layer. When the thickness of the Mackinawite layer passes a critical thickness, it further creates cracks within the corrosion product. These cracks act as roads that allow the solution to reach the metal-bulk solution inter-surface and also these cracks act as

reaction pathways to form excess iron sulfide. Figure 2.4 shows different reaction pathways that can be identified in grown Mackinawite layer [26].

Since the Mackinawite is a good electrical conductor, H_2S is reduced on the surface followed by the anodic reaction occurred at the metal surface. Reaction path (b) shows the metal surface that is underneath the Mackinawite layer. Formed Fe^{2+} at anodic sites can be traveled through the reaction pathway (e) which is shown in Figure 2.4.

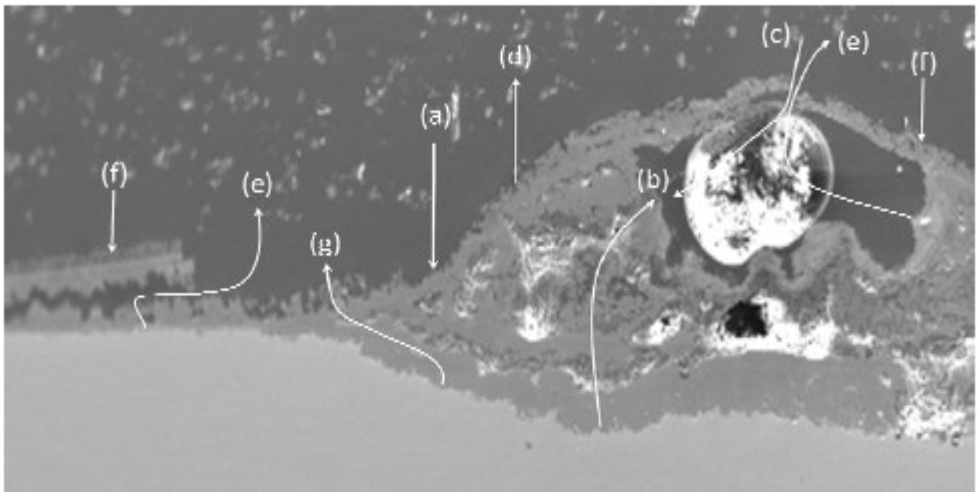

Figure 2.4: Possible reaction pathways for the formation of Mackinawite,

(a) Reduction of H_2S at the surface which results in the formation of hydrogen and adsorbed sulfide,(b) The location which acts as the anode ,(c) Diffusion of H_2S into voids that were formed due to the ruptures (d) Origin of Fe^{2+} due to film dissolution, (e) diffusion of soluble iron species through film ruptures to film/bulk interface,(f) precipitation of FeS the film surface, (g) diffusion of Fe^{2+} between planes of Mackinawite crystal as described under section 2.2, to reach film surface. [26]

At the same time HS^- and S^{2-}cations formed at Mackinawite surface can diffuse into the voids through the ruptured pathways as shown in pathway (c) of Figure 2.4. This mechanism causes to meet optimum conditions to form FeS through heterogeneous reactions as shown in equation 1 -5. Hence, FeS begins to form along the ruptures pathway. If Fe^{2+} ions do not meet cations to form FeS within the cracks, they move to

the film surface and form FeS. This is shown in path (f) in Figure 2.4. Figure 2.5 shows the precipitated new corrosion product on a crack mouth of a Mackinawite layer [27]. This precipitation of excess Mackinawite on the top of the film surface occurs due to the aforementioned mechanism. It is seen that FeS nucleates at the edge of the cracks.

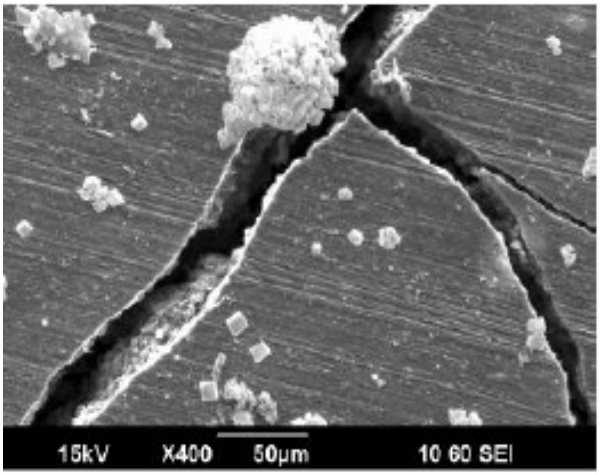

Figure 2.5: SEM image ruptured corrosion product layer. [27]

In addition to the aforementioned mechanism of formation of FeS precipitates within the cracks, there is another path to nucleate FeS [4]. This mechanism is defined with the aid of the Mackinawite sheet like structure. As it earlier mentioned, Mackinawite can adsorb divalent metallic cation. Once the metallic cations are adsorbed by a Mackinawite film, they are free to move through the spaces found in Mackinawite film. Generally Fe^{2+} ions migrate away from the metal surface and move toward the film-electrolyte boundary by moving along this path. If these Fe^{2+} ions find a crack, there is a possibility of formation of FeS within the crack. If Fe^{2}+ ions fail to find a crack while they are intercalated, FeS formation occurs at the film surface.

Therefore, when the ferrous ions in reaction path (b) find a film-electrolyte boundaries can be formed following three different mechanisms. First, the adsorbed sulfide in reaction path (c) together with those ferrous can be precipitated as FeS within the crack. Second, ferrous ion can diffuse out cracks to the film-bulk solution interface as shown by reaction path (e) or they can diffuse between the planes of the Mackinawite until they

reach a sulfide source at the film- electrolyte boundary to form one of the Fe-S species. Third, ferrous that diffuse out (f) the cracks to the film/bulk solution interface are also available to either enhance the local film growth or nucleate new FeS crystals, such as cubic FeS, troilite or pyrrhotite (path f).

If the Fe^{2+} ions released by the reaction reach the scale/electrolyte surface to form surface precipitates, at least one of four things occur. Either the existing Mackinawite film continuous to grow or new Mackinawite crystals precipitate near the crack mouth, cubic FeS crystals nucleate, needle-like troilite crystals nucleate or hexagonal plates of pyrrhotite nucleate. Of Course, there is also the possibility that solution manages to "capture" the newly produced ferrous ion and keep it in solution. In this case, nothing new will immediately form on the surface.

2.4 Identification of sulfide stress cracks

Sulfide stress cracks can be identified through visual observations if the cracks are propagated closer to the failure. The case study conducted by Ziaei et al [28], visually observed that sulfide stress cracks had been initiated always from surface pits. They conducted their case study on sulfide stress cracking of a wellhead flow control valve body categorized as A216-WCC. Figure 2.6 shows surface corrosion pits of a failed valve body.

Further, ziaei et al investigated a cross section of as received valve body after 36 months in wet H_2S environment. They noticed that crack had been initiated from the inner surface of valves surface that was in straight contact with hydrogen sulfide. The crack had penetrated 50% of the thickness of the valve body where the depth of corrosion were 15mm while the thickness of the valve body takes 30 mm. Figure 2.7 shows the image of the crack.

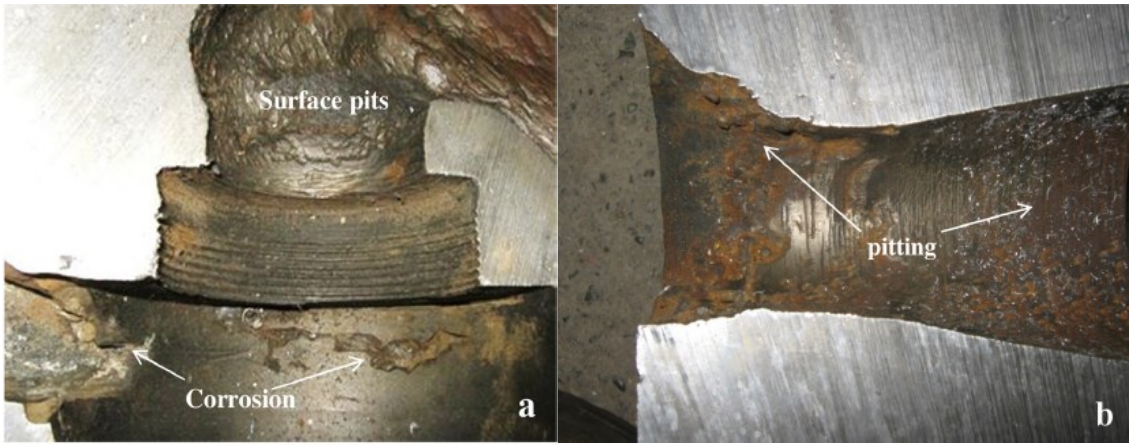

Figure 2.6: corroded inner surface of the control valve body, (a) near the seat ring and (b) near the valve's flange [28]

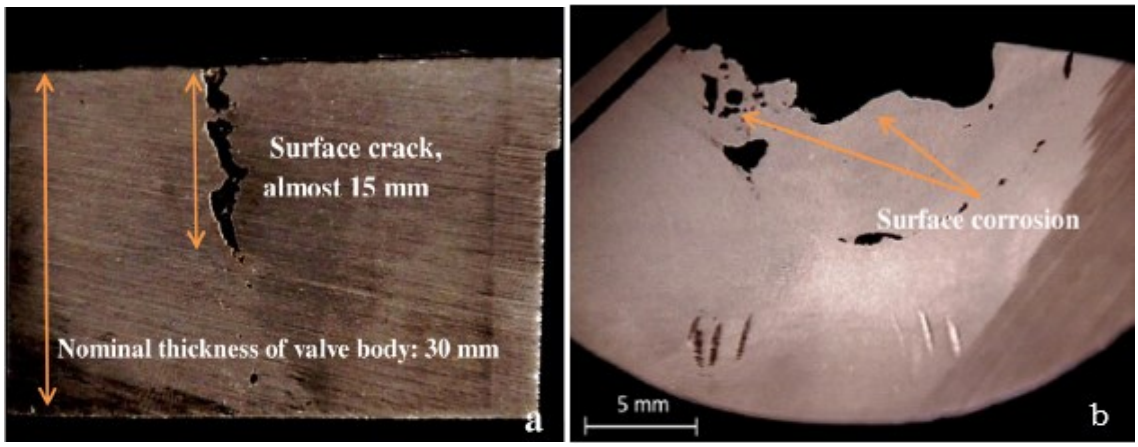

Figure 2.7: Corrosion cracks of the valve body base metal after 36 months of exposure in sour environment (H_2S rich) (a) initiation of cracks from inner surface of the valve's surface (b) surface corrosion cracks at the valve's flange. [28]

If the Sulfide stress corrosion cannot be visually observed, the best approach is observation of scanning electron microscope images. Figure 2.8 shows the Sulfide stress cracks observed through the scanning electron microscope at the case study conducted by Ziaei et al[28].

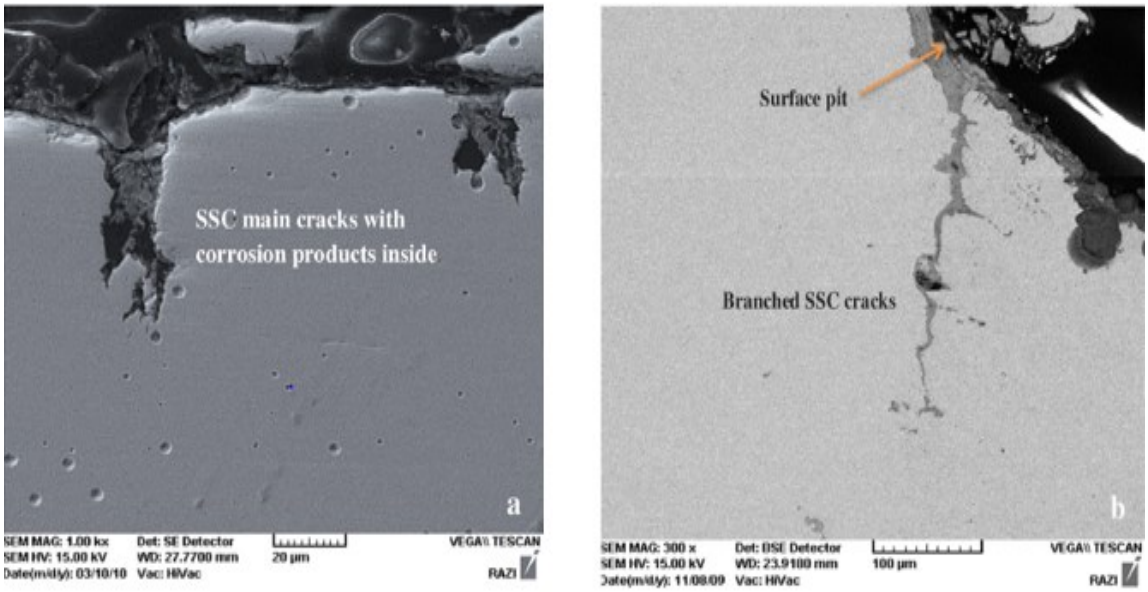

Figure 2.8: SEM images of SSC cracks in A216 steel (a) main crack and (b) branched cracks (similar to a tap root). Cracks propagated from inner surface to the base metal. [28]

Based on the SEM image analysis, they came to following conclusions regarding the sulfide stress cracks. Sulfide stress cracks consist of a multiple stress cracks. The main crack propagated from the metal surface perpendicular to the applied stress (Figure 2.8(a)). In addition to the main crack, at the metal surface, nucleation of micro cracks can be observed inside the metal. Crack propagation occurred making branches following the favorable orientations (Figure 2.8 (b)). The same case study caught an interesting observations interesting observations at sulfide stress cracks. It was observed that the existence of hydrogen induced cracks near the crack tip of the main SSC crack. Further, they mention that stress concentration at the inclusion or at matrix interface makes an ideal site for initiation of cracks and hydrogen trapping. Hydrogen molecules are formed at defect sites when the recombination of trapped hydrogen occurs. The pressure build up due to the formation of hydrogen molecule leads to the formation of cracks.

The research conducted by M. Liu[29] et al mentions that inclusions in a metal play a main role of initiation of hydrogen induced cracks and sulfide stress cracks. They mention that crack nucleation and propagation should be studied through microstructure

and crystallographic information of cracks. They suggests that optical microscope (OM), scanning electron microscope(SEM) and transmission electron microscope (TEM) are good techniques to study the microstructure while the electron backscatter diffraction is suitable for obtaining crystallographic information. The investigation has been carried out to study the crystallographic details within four areas. They are near crack which is shown in a black margined box, near crack branch which is shown in a red margined box, away from crack which is shown in a thick blue margined box and crack free which is shown in light blue margined box in Figure 2.9. It can be seen that the crack is consisted with several branches on both side of the crack.

The crystallographic information carried out by electron backscattered diffraction (EBSD) analysis technique for the aforementioned four different locations (Figure 2.9) showed a fixed relationship between each location and the spread of high-angle grain boundaries, medium-angle grain boundaries, and low-angle grain boundaries in the four regions. As a result, M Liu [29] observed that the number fraction of low angle grain boundaries is highest which takes 50% of total & of total in the region of near-crack. The scales of medium angle grain boundaries are possibly similar in the four regions but the percentage wise it gets a low value which is almost less than 15% of total compared to the high angle grain boundaries & low angle grain boundaries. In contrast, crack free region was the region where highest percentage of high angle grain boundaries were found.

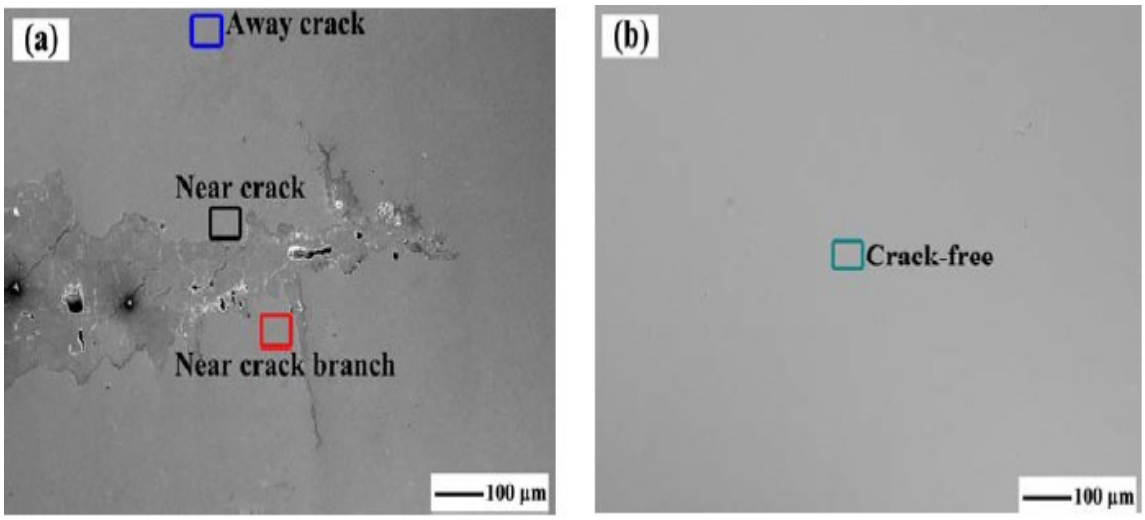

Figure 2.9: SEM images of the cross section plane of specimens and the selected areas for electron backscatter diffraction (EBSD) analysis. [29]

Jim gossett [7] in his article on detecting sulfide stress cracks explains that crack initiation always occur following the pit formations on the metal surface. Further, he stresses that cracks are propagated as a network of fine feathery, branched cracks rather than a propagation of single crack.

To detect sulfide stress cracks, several test methods have been defined based on different standards. Among them, standards of American Society for Testing and Material, American National standard institute, American Society of Mechanical Engineers and American Petroleum Institute are widely used.

ANCI/NACE TM0177-2016 is standard test method approved by American national standard. NACE international task group has published this standard in 1977. This standard has been moderated five times in 1986, 1990, 1996, 2005 and 2016.

The test method stands for the laboratory testing of metals for SSC and stress corrosion cracking (SCC) in H_2S surrounding. The standard is expected to be used by laboratory and materials personnel to maintain a compliance with SSC and SCC testing. It includes testing for the metals those are conducted using double-cantilever-beam (DCB), C-ring and tensile, bent-beam test specimens. The test method advices to conduct sulfide stress cracking tests at room temperature while the stress corrosion cracking tests are advised to conduct at elevated temperature.

2.5 Comparison of models

Number of models have been developed over past fifteen years to predict the behavior of sour corrosion. The developed models predict rate of hydrogen sulfide corrosion [12][13], failure stress due to sulfide stress cracking in terms of adsorbed hydrogen content in steel[3], distribution of hydrogen atoms at crack tip[30], crack growth rate and threshold stress intensities[31], dependency of threshold intensity on the local hydrogen concentration at the fracture process zone [32], amount of hydrogen embrittlement in terms of hydrogen concentration in the environment, stress intensity factor ,yield strength.[33].

However occurrence of Sulfide stress corrosion in a particular circumstance still cannot be predicted systematically [3]. Most of the models predict accurate results only under specific conditions. As examples, the model developed by sun et al [12] to predict the sour corrosion rate predicts accurate results when the time duration of corrosion is increased. Figure 2.10 shows how the model predicted values vary with time duration and H_2S concentration.

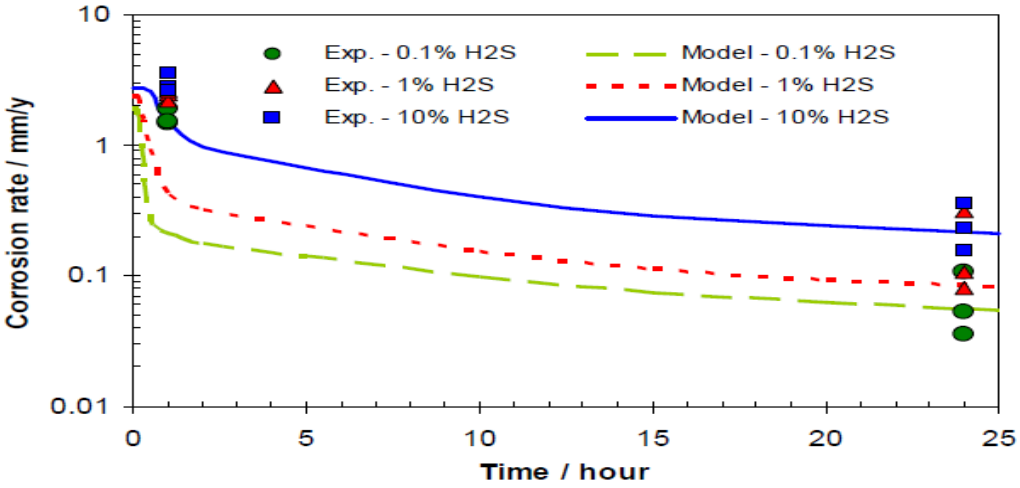

Figure 2.10: The experimental and prediction corrosion rate vs. time under the conditions of total pressure p=1 bar, H_2S gas concentration from 0.1% to 10%, T= 80°C, reaction time of 1 hour and 24 hours, pH 5.0-5.5, and velocity 0rpm[12]

The model developed by Zheng et al [13] tend to predict wrong results when the pH value get decreased and H_2S partial pressure in the environment get increased. Figure 2.11 shows the experimental and model predicted corrosion rates at pH 4 with H_2S partial pressure and Figure 2.12 shows the experimental and model predicted corrosion rates at pH5 with H_2S partial pressure.

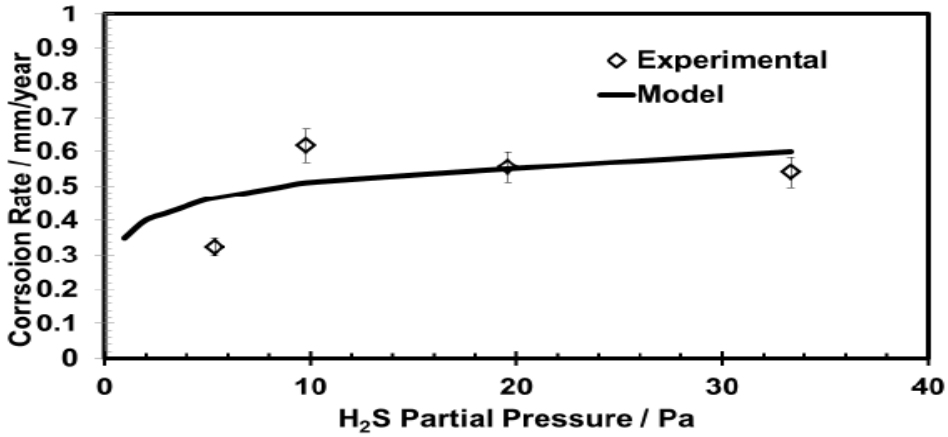

Figure 2.11: Experimental corrosion rates and Model predicted corrosion rates under different partial pressures of H_2S where pressure = 0.1Mpa, pH = 5, temperature = 20 ºC.Data taken from Lee [34].

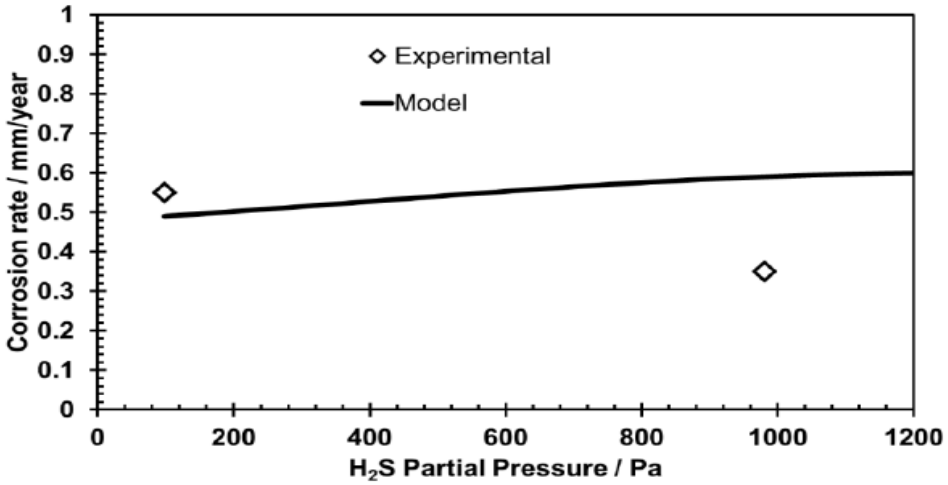

Figure 2.12: Experimental corrosion rates and Model predicted corrosion rates under different partial pressures of H_2S where pressure =1Mpa, pH = 4, temperature = 25ºC.Data taken from Choi et al.

It can be seen that when the H_2S partial pressure get increased at pH 4, model predicted corrosion rate gets deviated from the experimental value. But model predicted corrosion rates and corresponding experimental corrosion rate are in a good agreement under all of the H_2S partial pressure values.

However the experiment conducted by serebrinsky et al [33] could predict the extent of hydrogen embrittlement as the prediction are in good agreement with all of the available measurements. But that model is not predicating the sulfide stress corrosion directly. Instead it discusses the phenomenon of general hydrogen embrittlement. Asahi et al [3] directly discusses the prediction of SSS in high strength tubulars. The model predict the failure stress in terms of adsorbed hydrogen content to the metal. But surprisingly, the investigation hind the validation part.

Since the developed models are not accurate enough to predict the sulfide stress corrosion, industry is still lacking of an applicable prediction model. As an overall study it can be concluded that the models are predicting wrong results as they are considering irrelevant and less significant factors at developing stage. Therefore the factors effecting the behavior of sulfide stress corrosion is much important to be discussed.

2.6 Factors effecting sulfide stress cracking.

The literatures states that the sulfide stress corrosion is mainly governed by the type of material, pressure/tensile stress, H_2S concentration, Hydrogen ion concentration (pH value), temperature of the environment, time duration, flow effects solution composition and other chemicals[1][3]. It can be seen that these factors are similarly effect on the other types of hydrogen assisted cracking mechanisms. Although these factors are considered as the governing factors of sulfide stress cracking phenomena, all factors are not effecting equally likely on the behavior of corrosion.

H_2S concentration and pH value can be identified as a major factor that effects the behavior of sulfide stress cracking [34][35][36]. Morana et al [37] conducted an experiment to study the SSC resistance of high-strength carbon steels (P-110, Q-125, Grade 140 and 150) by varying pH and H_2S partial pressure from 3.5 to 5.5 and 0.015 to 7.25 psi, respectively. The test results for p-110 steel showed that steel can survive for 75 hours without a failure at 7.25 psi partial pressure of H_2S at pH 5.5. But it was detected that the steel can survive up to 720 hours when the partial pressure of H_2S was decreased systematically. However it was noticed that when the pH value was decreased

from 5.5 to 3.5, susceptibility for SSC was increased even at low H_2S partial pressure. Q-125 steel showed the same trend as p-110. Figure 2.13 displays the SSC behavior of the tested specimens in terms of pH and H_2S partial pressure. It provides safety windows where the steel grades can be used for downhole operation without concern of SSC failure. The overall results of the study indicated that SSC susceptibility of a metal increases with reduction in solution pH and increase in H_2S concentration.

Cancio et al states in their experiment [38] that the concentration of H_2S in the testing solution affects both the value of critical stress intensity factor (K_{ISSC}) and its relation with temperature. Low amounts of H_2S increase K_{ISSC} and at the same time reduce its dependence with temperature. Further it says, lowering pH and H_2S partial pressure increases K_{ISSC} (for the same initial applied intensity factor) and at the same time increase hydrogen absorbed concentration. They stress that SSC resistance and absorbed hydrogen concentration are inversely related.

The other significant factor that effects the behavior of sulfide stress cracking can be identified as the applied stress on steel. The term of applied stress converts to hydrostatic pressure when it is applied to pipeline steels [39]. Hirth [40] in his experiment, mentions that there is a strong relationship between hydrostatic stress and hydrogen penetration into steel as shown in equation 4.

$$C_H = C_0 \exp\left(\frac{\sigma_h V_H}{RT}\right) \quad \ldots 4$$

Where, C_H is the hydrogen concentration after hydrogen penetration. C_0 is the initial hydrogen concentration. T is the absolute temperature, R is the gas constant, V_H is the partial molar volume of hydrogen and σ_h is the hydrostatic stress.

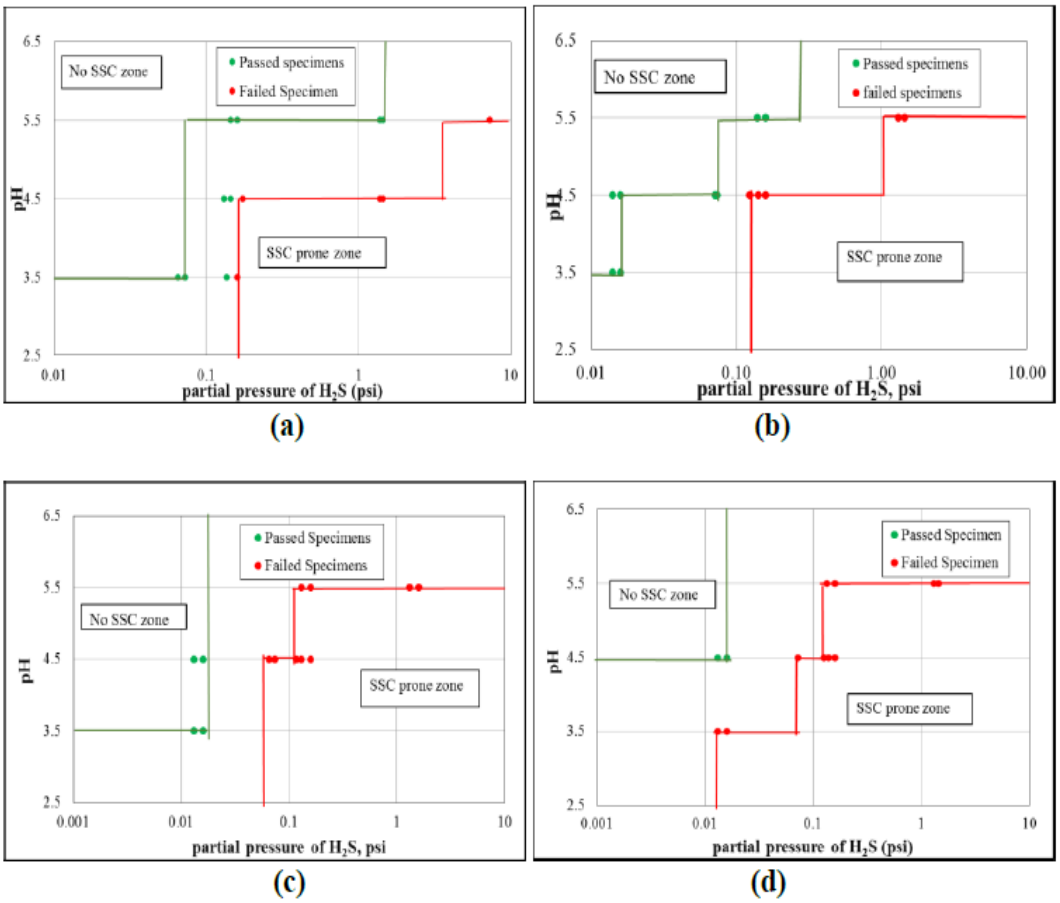

Figure 2.13: SSC failure windows for pH and H_2S partial pressure (Tale (2014) redrawing from Morana and Nice (2009)): a) P-110; b) Q-125; c) Grade 140; and d) Grade 150 [37].

Zhao et al [39] conducted an experiment to investigate the resistance of SSC in pipeline steels considering two factors which are applied stress and microstructure. Single-edge notched tensile method was undertaken in the experiment. The failure time was measured using set of specimens which were uploaded under the selected applied stress. Micro alloy steel samples (named as A) and non - micro alloy steel samples (named as B) were selected to prepare test specimens where three types of microstructures of Acicular ferrite (AF), aged acicular ferrite (AAF), ferrite-pearlite (FP) were experimented for each steel type. Figure2. 14 shows the experimental results carried out by Zhao [39] to express the relation between applied stress and fail time. It can be seen

that when the applied stress is increased, time taken for failure drastically reduces for all steel samples. Therefore it was concluded that the propagation of SSC and applied stress has a positive relationship.

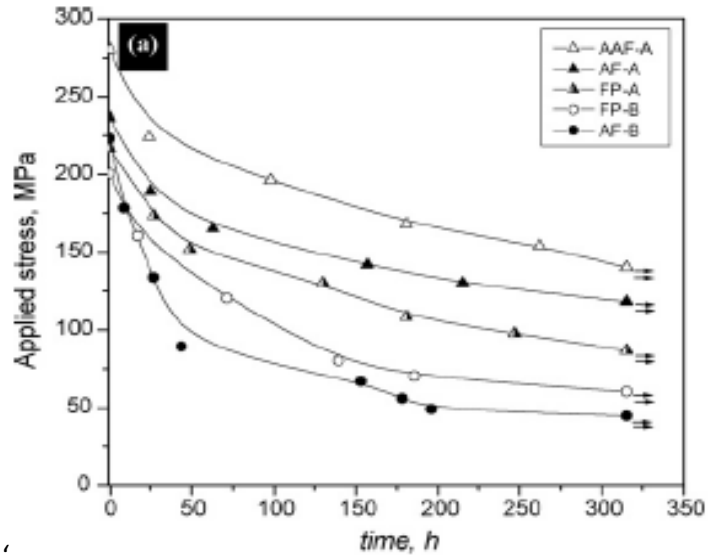

Figure 2.14: Relation between applied stress and fail time [39]

Time duration can be identified as the third significant factor that effect sulfide stress corrosion. Aviles et al conducted an experiment to investigate the corrosion resistance and hydrogen induced cracking susceptibility of API 5L X65 and API 5L X80 Steels at H_2S environment [41]. The research was conducted under two methodologies where one was conducted in de-aerated or in H_2S saturated solution for 1 hour (Experimental procedure 1) and the other one was conducted only in H_2S saturated solution for 24 hours(Experimental procedure 2). In both the methodologies, open circuit potential (OCP) was measured following electrochemical impedance spectroscopy (EIS) and potentio-dynamic polarization test (PDP). According to the authors, the mechanism of corrosion reactions was same at short duration test as well as at long duration test. This was proven through the characteristics of the EIS experimental diagram. It was seen that EIS characteristics were same for all the samples irrespective of time duration. However, both the materials indicated a reduction of the intensity of corrosion where this conclusion were carried out through an observation of the increment in impedance as a

function of immersion time. Figure 2.15 shows the EIS diagrams carried out for 1 hour and Figure 2.16 and Figure 2.17 shows EIS diagrams carried out for 24 hours.

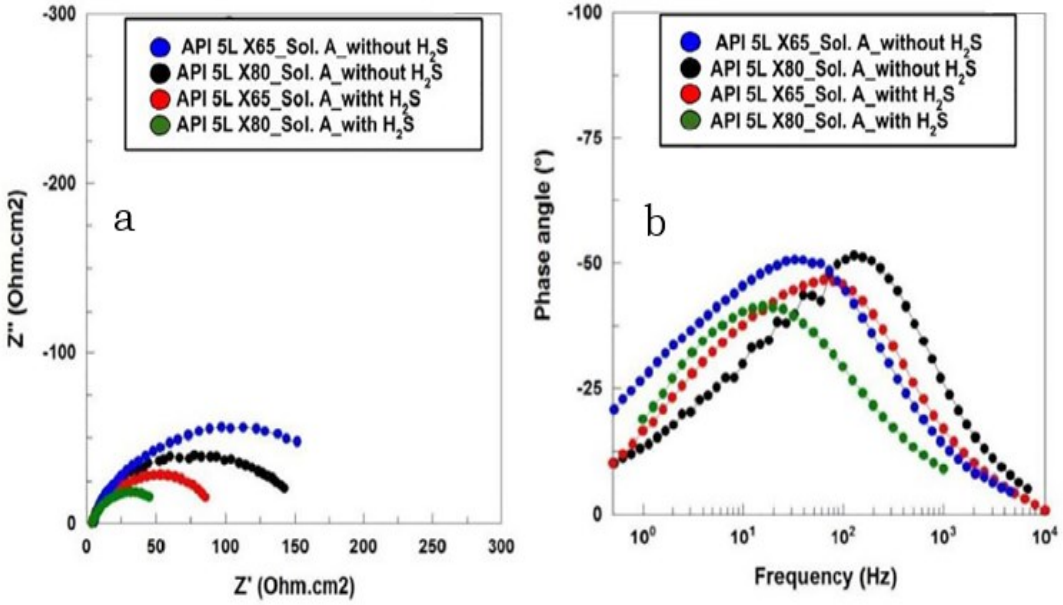

Figure 2.15: (a) phase angle (b) diagrams of API 5L X65 and API 5L X80 steels in de-aerated solution A, NACE TM0284 (2011), without and with H_2S saturation. [41]

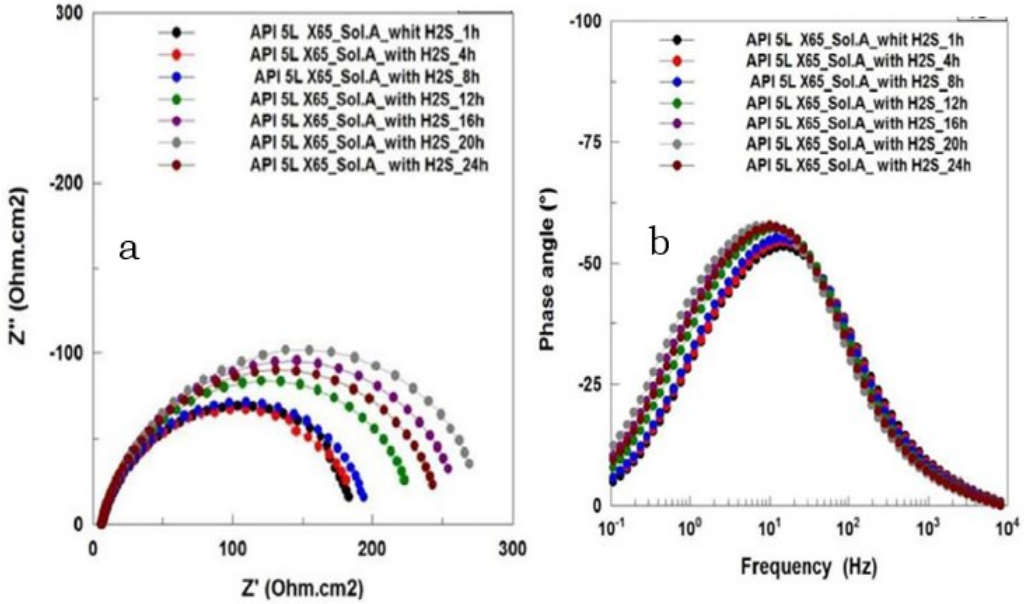

Figure 2.16: (a) phase angle (b) diagrams for the API 5L X65 steel during 24h immersion in de-aerated solution A, NACE TM0284 (2011), saturated with H2S, sour medium. [41]

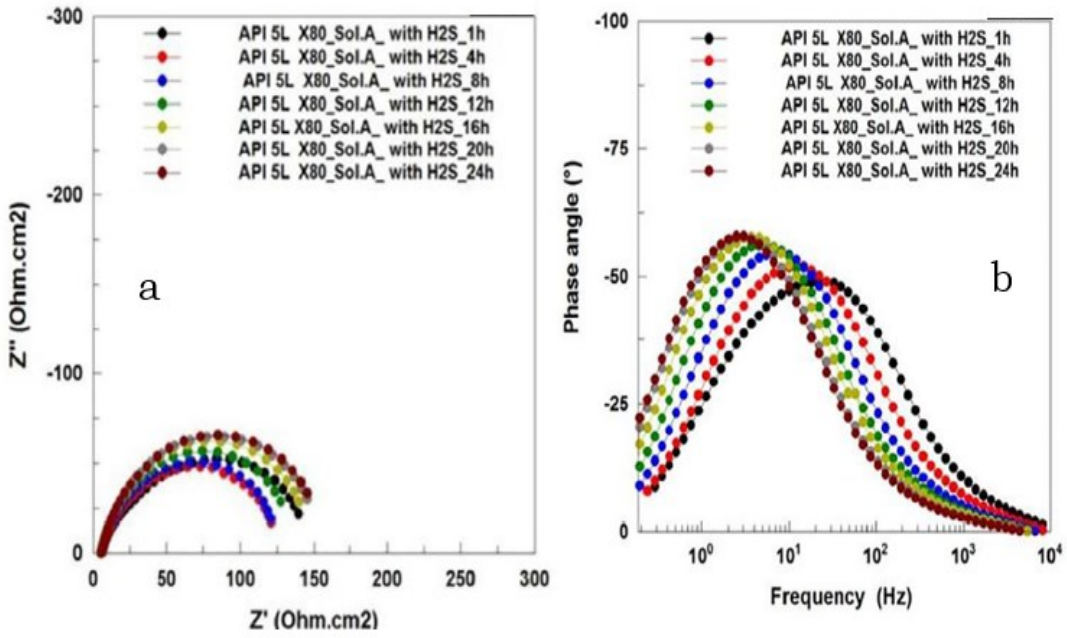

Figure 2.17 : (a) phase angle (b) diagrams for the API 5L API 5L X80 steel during 24h immersion in de-aerated solution A, NACE TM0284 (2011), saturated with H2S, sour medium.[41]

As Aviles et al [41] says, most of the sour corrosion research states that the corrosion rate or intensity of corrosion attack decreases with increasing time duration of sulfide stress corrosion. Smith [1] mentions, in CO2/H2S corrosion, the corrosion rate had been observed to be high initially, and then drops off significantly at longer time. Smith elaborate that the reason for this behavior is formation of iron sulfide scales. Iron sulfide layers that were formed on the steel surface act as a barrier for reactants and hydrogen irons to enter the steel.

There is a lack of researches that have been carried out to study the influence of time duration on the behavior of sulfide stress cracking. However, it can be getting an understanding of the effect of time duration through some of the experiments that were conducted to measure the effect of other parameters such as H_2S concentration, pH value and hydrostatic pressure etc.

The research conducted by Tumuluru [42] on Sulfide Stress Corrosion Cracking in low-Alloy Steel Inertia Friction Welds plot a graph of time to failure due to the sulfide stress

cracking vs applied stress. The metal samples had been made out of AISI 4137-H steel. The SSC test specimens from the welds were loaded from 103.4 MPa to 206.8 MPa at increments of 34.5 MPa (5000 psi) and from 206.8MPa (30,000 psi) to 413.7 MPa (60,000psi) at 68.9 MPa (10,000 psi) increments. The SSC test specimens machined along the transverse direction of AISI 4137-Hsteel were loaded from 137.8 MPa (20,000 psi) to 413.7 MPa (60,000 psi) at increments of 34.5 MPa (5000 psi). The time to failure was noted in each case. According to the figure 2. 18, plots were made between the loading stress (applied stress) and the time to failure for the welds and AISI 4137-H steel in the transverse direction. It can be concluded from the plot that the time duration for a failure due to SSC depends on the applied stress. Therefore the effect of time duration on the behavior of SSC depends upon the applied stress.

As a factor, temperature determines whether SSC occurs or SCC occurs in sour environments. SSC tend to occur at low temperature and SCC tend to occur at high temperature under the same environment [3].

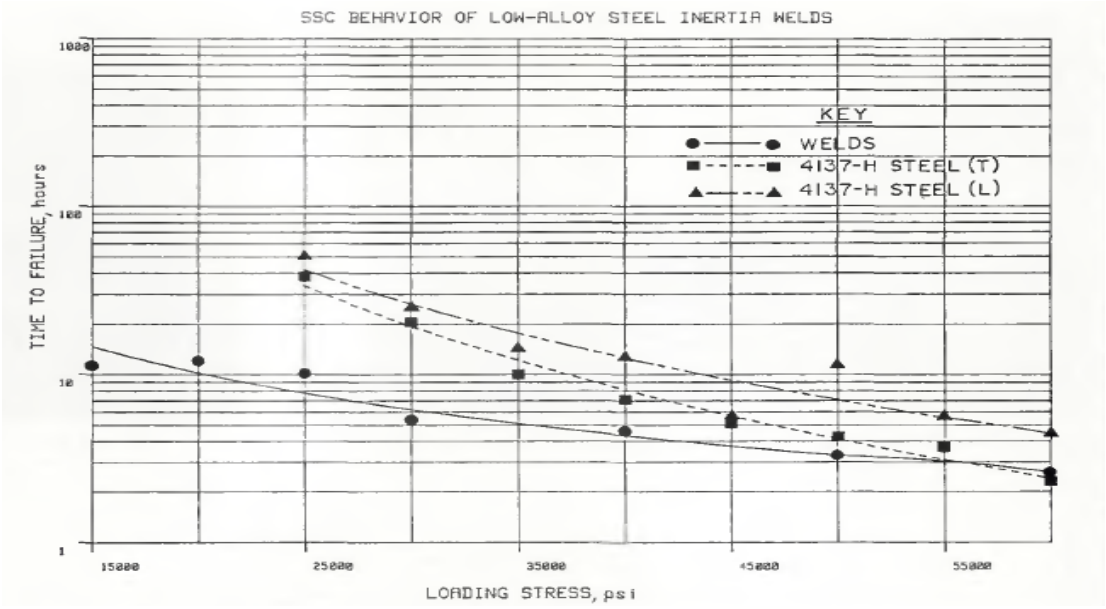

Figure 2.18: Loading stress vs. time to failure plots for the inertia friction welds and AISI 4137-H steel [42]

3 EXPERIMENTAL PROGRAM

3.1 Material

API 5L grade B steel used for all experiments were procured from Sri Lanka Petroleum Corporation in the form of a seamless pipe of 1m in length with a thickness of 11mm and a diameter of 168 mm. The chemical composition was verified by atomic emission spectroscopy test (Table 3.1). Table 3.2 shows mechanical and physical properties of API 5L Grade B steel in accordance with the API 5L grade B steel specification [48] [49].

Table 3.1: Chemical composition of API 5L GradeB

Element	Mass Fraction (%)	Max Allowed Weight Fraction (%)
Fe	98.600	Not specified
C	0.201	0.28
Si	0.292	Not specified
Mn	0.470	1.20
P	0.029	0.030
S	0.007	0.030
Cr	0.059	0.5
Ni	0.103	0.5
Al	0.043	Not specified
Cu	0.001	0.5

Table 3.2: Mechanical and physical properties of API 5L Grade B steel

Mechanical/Physical property	Value or percentage (Minimum)
Tensile strength	415Mpa
Yield Strength	245Mpa
Elongation	19.68 %
Density	7850 Kg/m^3

3.2 Experimental setup – Test conditions in the corrosive vessel

Experimental setup is consisted with three main components. They are test vessel, test specimens and sample holder. The experimental setup was designed in accordance with ANSI/NACE TM0177-2016standard test method.

3.2.1 Fabrication of the test vessel and specimens

The test vessel was design adhering to the following key points stated in the standard.

- Test vessel was allowed to be constructed considering the placement of test specimens. The size of test vessel was determined considering the required solution volume. Shape shall be determined considering the nature of test fixtures which are used to apply the tensile stress to test specimens and entry ports of the test solution.
- Test fixtures and test specimens should be designed to overcome the other types of corrosions. Electrical isolation of test specimen from test vessel and test fixtures are highly recommended.
- Galvanic coupling in the test vessel must be avoided at any place.

The test vessel was made out of 5mm thick acrylic sheets where the chamber was sealed by the application of silica glue. Silica glue was used to avoid the contact between the acrylic glasses and the test fixtures. The door of the test vessel was kept fixed using 6mm diameter threaded bars (Figure 3.1).The test vessel was tested for leaks with N_2 gas at 1.5 atm.The total volume of the test vessel was maintained to 2856 cm^3 while the volume of the test solution was 2000 cm^3 (70.0 % of the volume of test vessel) [43]. The test vessel was sealed to prevent the leakage of solution and gases.

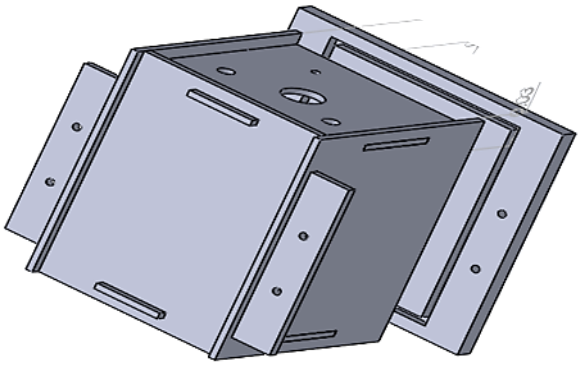

Figure 3.1: Test vessel

3.2.2 Test solution

The test solution was maintained at 24 ºC ± 3 ºC in the test vessel. Since the pH value of the test solution was maintained at 2.7 and 3.5, two test solutions were used as per the standard. The standard introduces four test solutions of test solution A, test solution B, test solution C and test solution D. The test solutions A and B were used to maintain pH values of 2.7 and 3.5 respectively.

Test solution A

Test solution A is an acidified H_2S – saturated aqueous brine solution. The solution was a mixture of 5.0wt % sodium chloride, 0.5wt% glacial acetic acid and deionized water. While the pH value is decreased over the time, H_2S purging should be controlled when pH value gets closer to 2.6 and should be stopped at 2.7. pH value was maintained at 2.7 when it was in the test vessel.

Test solution B

Test solution B is an acidified and buffered H_2S – saturated aqueous brine solution. The solution was a mixture of 5.0wt% sodium chloride, 2.5wt% glacial acetic acid, 0.41wt % sodium acetate and deionized water. While the pH value is decreased over the time, H_2S purging should be controlled when pH value gets closer to 3.4 and should be stopped at 3.5.pH value was maintained at 3.5 when it was in the test vessel.

Each test solution was de-aerated at a rate of 100 ml/min by N_2 gas for 1 hour. Test vessel was also de-areared in the similar manner before the test solution enters the test vessel. The test solution was allowed for testing if it showed a full transparent solution when it was in the test vessel.

3.2.3 Test specimen

The configuration of the test specimen was designed for fit-for- purpose testing as it agreed with the standard. Figure 3.2 shows the schematic diagram of the designed test specimen. Since overheating and cold working can affect the original properties of steel, machining of test specimens gauge section was carefully done. The final surface finish was achieved through the mechanical polishing that was done using 0.25 µm grit papers. Before testing, test specimens were cleaned with alcohol and washed off with acetone. Just after the cleaning process finished, the test specimen was fixed in the vessel avoiding any contamination in the gauge section of the test specimen.

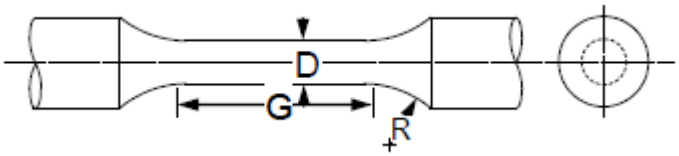

Figure 3.2: Dimensions of the Test specimen.
Where, G = 55.00mm, D = 6.72mm, R = 1.00mm

3.2.4 Sample holder/Specimens fixture

The sample holder (Figure 3.3) was made out of mild steel and it was fully coated by an epoxy coating to mitigate the influence of galvanic corrosion. The sample holders were used to apply a tensile load as per the test method A, mentioned in the standard. Predetermined loads were applied to each specimen before the solution was entered. Three test specimens were placed within the stress fixtures for a specified test.

3.2.5 Determination of the applied load (tensile) values.

The values of tensile loads for the application of test specimen were back calculated in accordance with the standard ASME B31.4-2002[44]. Formula 5 was used for the determination of applicable allowable stress corresponding to internal pressures. Formula 6 was used to determine the applicable tensile load of the test specimen.

$$s_H = \frac{p_i d}{2t} \qquad \ldots 5$$

Where S_H = the applicable allowable stress value, P_i = internal gauge pressure, t = the wall thickness of the pipeline (11 mm), d = the outer diameter of the pipeline (168.3mm). Since the internal pressures of transmission sour pipe lines are maintained at high values (200 – 1500 psi)[45], three corresponding tensile loads for the application of test specimen were calculated for 200psi, 300psi and 400 psi internal pressure values.

$$F = P \times A \qquad \ldots 6$$

Where F = the applied load (tensile), P= applicable allowable stress value calculated by formula 5, A = the cross sectional area of the gauge section of test specimen (35.48 mm^2).

3.2.6 Final experimental setup

Figure 3.4 shows the final experimental setup which was ready for the corrosion test. The setup is comprised with mainly the test specimen, sample holder and test vessel. In addition to that the whole apparatus was covered with a plastic box to avoid the effect of environmental changes.

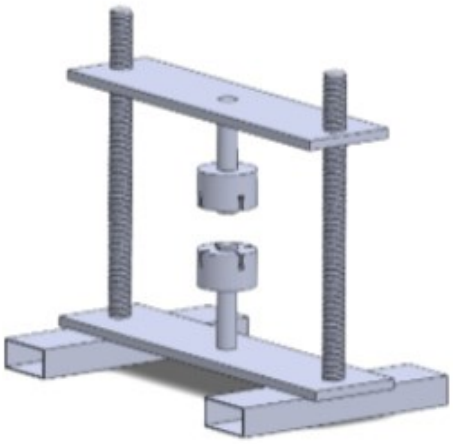

Figure 3.3 : Steel sample holder

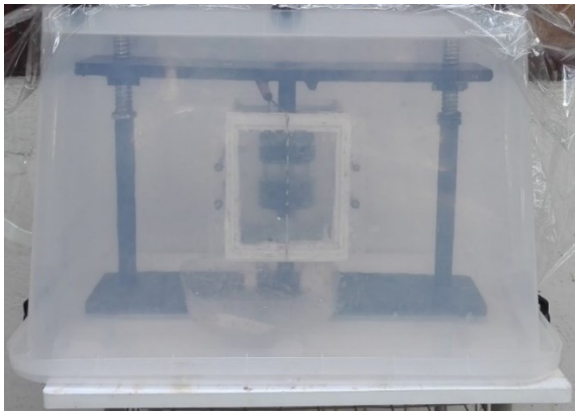

Figure 3.4 : Final Experimental setup

3.2.7 Experimental conditions.

Tensile loaded specimens were subjected to be corroded under 18 different test environmental conditions. The test environmental conditions were varied depending on the different combinations of time duration, applied load and the pH value of test solution. Temperature and the pressure were maintained at 27 ^{0}C and 1atm respectively. Table 3.3 shows the 18 different environmental conditions considered at the test.

Table 3.3 : Test environmental conditions

Test No.	Applied load (N)	pH value	Time duration (days)
1	400	2.7	15
2	600	2.7	15
3	800	2.7	15
4	400	3.5	15
5	600	3.5	15
6	800	3.5	15
7	400	2.7	30
8	600	2.7	30
9	800	2.7	30
10	400	3.5	30
11	600	3.5	30
12	800	3.5	30
13	400	2.7	45
14	600	2.7	45
15	800	2.7	45
16	400	3.5	45
17	600	3.5	45
18	800	3.5	45

3.2.8 Determination of depth of corrosion by SEM observations.

The specimens corroded under 18 test conditions were prepared for SEM observations. Observations were performed by the SEM model SEM- ZEISS, EVO18 – Research, Germany under BSD and SE modes, 20kV and 10 kV EHT values with 100µA current. The magnification was determined based on the crack length. The minimum magnification obtained was 250× while the maximum magnification was 1.5k×.

At the end of the specified time duration, each specimen was taken out from the test vessel and washed with DI water. Then each test specimen was cut transversely from three different places to obtain three different cross sections [Figure 3.5] using low speed precision cutting machine under the speed level 3 [Figure 3.6].

Each cross sections were ground by the grit papers numbered as 240,360,400 and 1200, following the stated order. Then they were polished using 1μm diamond solution. The prepared cross sections of specimens were observed by scanning electron microscope. From each specimen, the maximum depths of corrosion were identified.

Corresponding depth of sulfide stress corrosion for a specified test environmental condition was determined following the procedure mentioned below.

Firstly, a prepared cross section of a test specimen that was corroded under a predetermined and specified test environmental condition is observed through the scanning electron microscope. Secondly three maximum depths of corrosions were identified from three different places of the cross section. Considering the three maximum depths of corrosion, an average depth of corrosion value is defined for the considered test specimen. Figure 3.5 illustrates the measurement of three depths of sulfide corrosion values and calculation of average depth of sulfide stress corrosion value for a selected specimen. Since there were three specimens were corroded under a specified test environmental condition, three average depth of corrosion values were obtained for three specimens. Considering the average value of previously calculated three averaged depths of corrosion, the depth of sulfide stress corrosion is defined for the considered test environmental condition. 18 depths of sulfide stress corrosion were calculated for 18 different test environmental conditions following the aforementioned procedure.

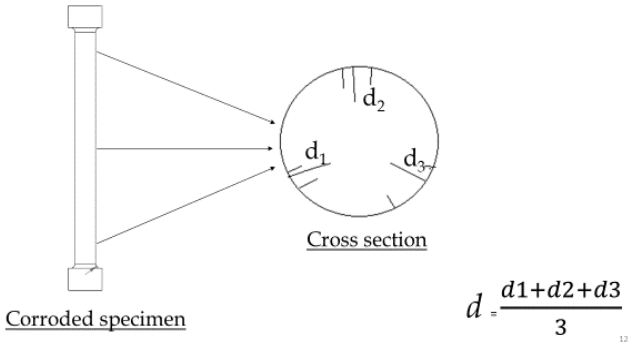

Figure 3.5: Three transverse cuts of a specimen and obtaining average depth of corrosion

3.2.9 SEM/EDAX analysis of SSC cracks

The SCC cracks were further analyzed using elemental profile lines. The distribution of Sulphur within the crack surface was investigated using this techniques.

Figure 3.6: Low speed precision cutting machine

3.2.10 Development of the statistical model

The statistical model was developed using SPSS (Statistical Package for the social sciences) software. The model predicts the depth of corrosion of sulfide stress corrosion as a function of time duration, pH value of the solution and the applied load. The depth of corrosion values measured under 18 test conditions mentioned in table 3.3 were entered to the software as the first step. Figure 3.7 and 3.8 show the data view and variable view of input of data to the software.

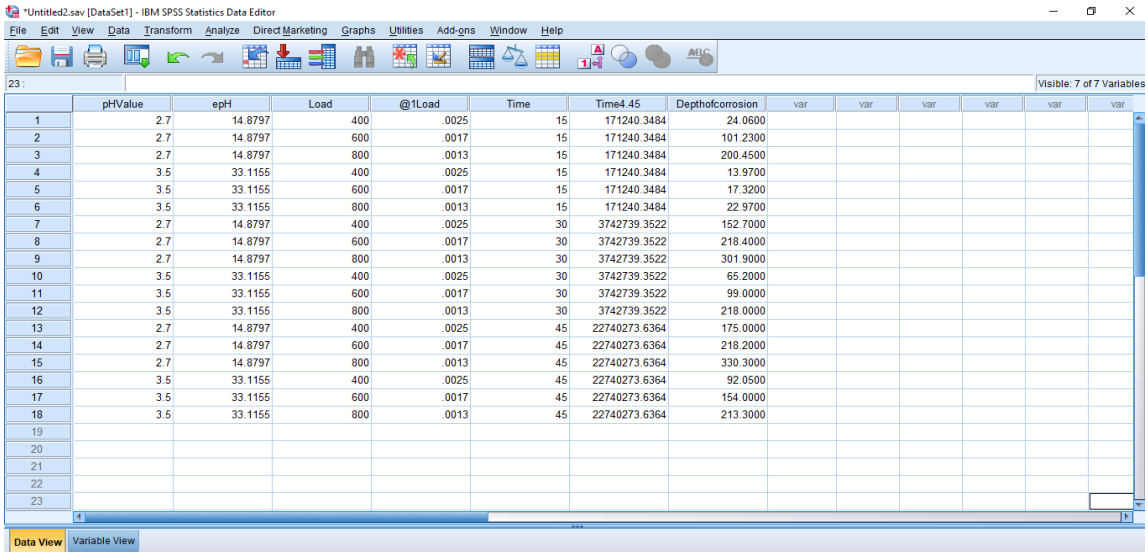

	pHValue	epH	Load	@1Load	Time	Time4.45	Depthofcorrosion
1	2.7	14.8797	400	.0025	15	171240.3484	24.0600
2	2.7	14.8797	600	.0017	15	171240.3484	101.2300
3	2.7	14.8797	800	.0013	15	171240.3484	200.4500
4	3.5	33.1155	400	.0025	15	171240.3484	13.9700
5	3.5	33.1155	600	.0017	15	171240.3484	17.3200
6	3.5	33.1155	800	.0013	15	171240.3484	22.9700
7	2.7	14.8797	400	.0025	30	3742739.3522	152.7000
8	2.7	14.8797	600	.0017	30	3742739.3522	218.4000
9	2.7	14.8797	800	.0013	30	3742739.3522	301.9000
10	3.5	33.1155	400	.0025	30	3742739.3522	65.2000
11	3.5	33.1155	600	.0017	30	3742739.3522	99.0000
12	3.5	33.1155	800	.0013	30	3742739.3522	218.0000
13	2.7	14.8797	400	.0025	45	22740273.6364	175.0000
14	2.7	14.8797	600	.0017	45	22740273.6364	218.2000
15	2.7	14.8797	800	.0013	45	22740273.6364	330.3000
16	3.5	33.1155	400	.0025	45	22740273.6364	92.0500
17	3.5	33.1155	600	.0017	45	22740273.6364	154.0000
18	3.5	33.1155	800	.0013	45	22740273.6364	213.3000

Figure 3. 7 : Interface of the data view of input of data

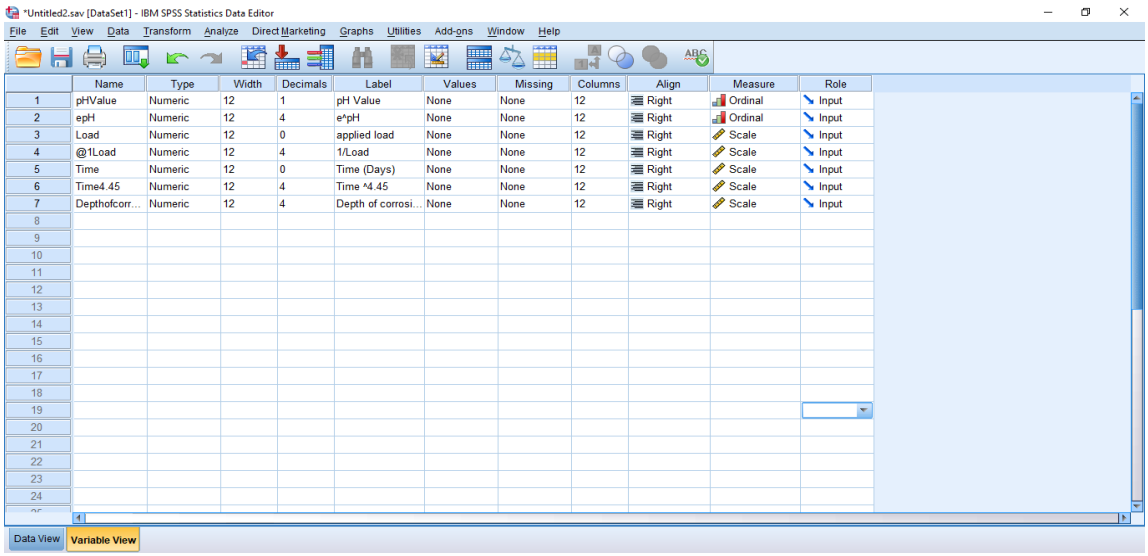

Figure 3. 8 : Interface of the variable view of input of data

At the development stage of the model, it was assumed the linear relationship, no auto correlation and homoscedasticity, no or little multicollinearity, multivariate normality [46]. The depth of corrosion was considered as the dependent variable of the model while the time duration, P_H value and applied load were considered as independent variables. The model was developed by multiple linear regression analysis. The multiple linear regression analysis was selected over nonlinear regression analysis as the model becomes simpler to be used.

Linearity between independent and dependent variables is a must in multiple linear regression analysis. The outliers were ignored since outlier effects are badly affecting on multiple linear regression analysis. Scatter plots were carried out for the testing of linearity. As the dependent variable was not linearly related with some independent variables, a non-linear transformation was carried out.

As the multiple linear regression analysis is valid only when the residuals arenormal, histogram and p-p plots were used for the examination of normality.

Multicollinearity was checked against four tests mentioned below.

- Correlation matrix –Correlation coefficients of Pearson's Bivariate Correlation matrix within all independent variables should be less than 0.08.
- Tolerance – Tolerance encounter the effect of a selected independent variable on all other independent variables. If the tolerance values are greater than 0.1, it can be concluded that there is no multi-collinearity in the data. If tolerance values are greater less than 0.1, there is a little probability of having multicollinearity in data. If the tolerance values are less than 0.01, multicollinearity must be presence in the data.
- Variance Inflation Factor (VIF) – VIF of linear regression is considered as the reciprocal of tolerance (VIF = 1/T). If VIF is greater than 10, it is considered that multicollinearity presence in the data.
- Condition Index – Condition index is calculated based on a factor analysis on independent variables. If the condition index of a data set gets values from 10 -30 implies that there is a little multicollinearity in regression variables. If the condition index is greater than 30, the data set cannot be accepted for multiple linear regression analysis since it indicates higher multicollinearity.

The Durbin Watson test were carried out to check the autocorrelation. Very small amount of autocorrelation in the data facilitates for the multiple linear regression analysis. If the residuals of the data set in multiple linear regression analysis are not independent from each other, autocorrelation may presence. When this phenomena is expressed using function notation, it can be stated that y(x+1) should be independent of y(x) to minimize autocorrelation. Homoscedasticity is the last assumption made in multiple linear regression analysis. This was checked using scatter plots in the focused research.

4 RESULTS AND DISCUSSION

4.1 Implementation of the model

The developed statistical model predicts the depth of sulfide stress corrosion in terms of time duration, pH value and applied load as expressed in the following formula.

$$DoC = -5.035e^{pH} - \frac{95455.143}{Applied\ Load} + 4.333 \times 10^{-6} \times Time^{4.45} + 400.140$$

Where,

DoC = Depth of sulfide stress corrosion in micro meters.

Applied load = Applied load on the test specimen in N

Time =Time duration in days that the specimen has been exposed to the test environment

pH = Average pH value of the test solution.

The implemented empirical formula was subjected to a series of statistical tests to confirm whether it satisfies the initial assumptions made. Figure 4.1, Figure 4.2 and Figure 4.3 show the scatter plots of depth of sulfide stress corrosion vs 1/applied load, depth of sulfide stress corrosion vs e^{pH} value and depth of sulfide stress corrosion vs $Time^{4.45}$ respectively. Each scatter plots was obtained to check the linearity between independent variables and the dependent variables. It can be seen that the depth of sulfide stress corrosion vs 1/applied load and depth of sulfide stress corrosion vs e^{pH} scatter plots have negative linear relationships while the depth of sulfide stress corrosion vs $Time^{4.45}$ has a positive linear relationship.

Figure 4.4, Figure 4.5 and table 4.1 stand for the normality test of the model. The histogram (Figure 4.4) shows a normal bel curve shape indicating that the all standardized residuals are normally distributed in the model. The p-p plot (Figure 4.5) indicates that the expected cumulative probability vs observed cumulative probability plot lies along the normal line. The linear behavior of the model was further confirmed

by Shapirowilk p values which are shown in table 4.1. It can be seen that the p values obtained for standardized residuals and unstandardized residuals are equal to each other. Further, based on the null hypothesis of H_0 – depth of corrosion is normally distributed in the population and the alternative hypothesis of H_1 – depth of corrosion is not normally distributed in the population, at 5% significance level, since the asymptotic significance is greater than 5%, the null hypothesis is not rejected and can be concluded that the dependent variable is normally distributed in the population.

Table 4. 1: Test of normality.

	Shapiro-Wilk		
	Statistic	df	sig
Unstandardized Residual	0.974	18	0.867
Standardized Residual	0.974	18	0.867

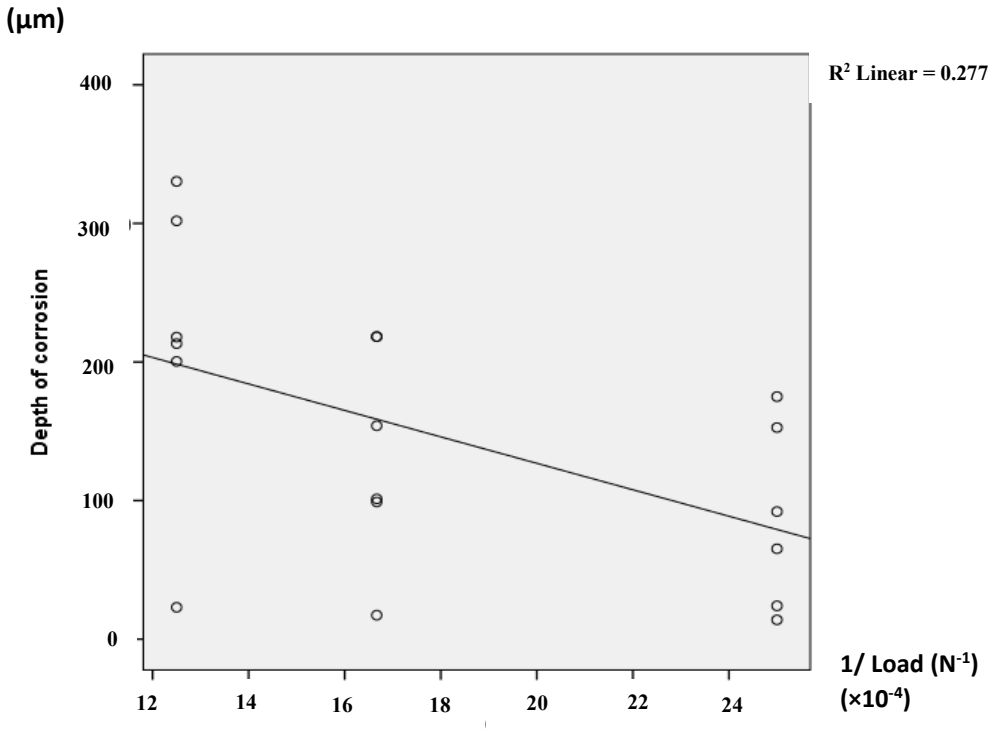

Figure 4. 1: scatter plot of depth of sulfide stress corrosion Vs 1/applied load

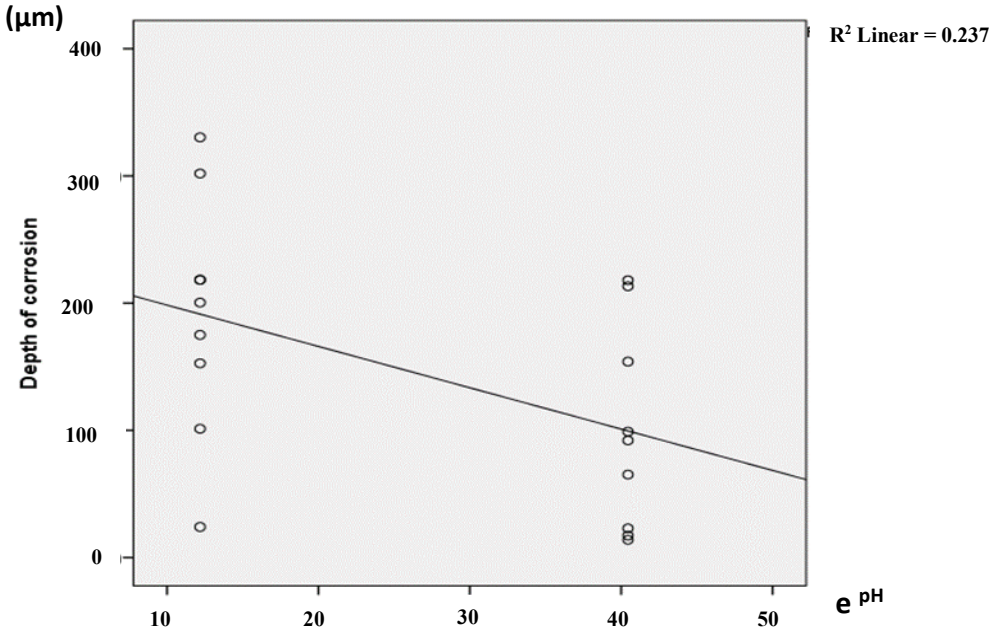

Figure 4.2: scatter plot of depth of sulfide stress corrosion Vs e^{pH} load

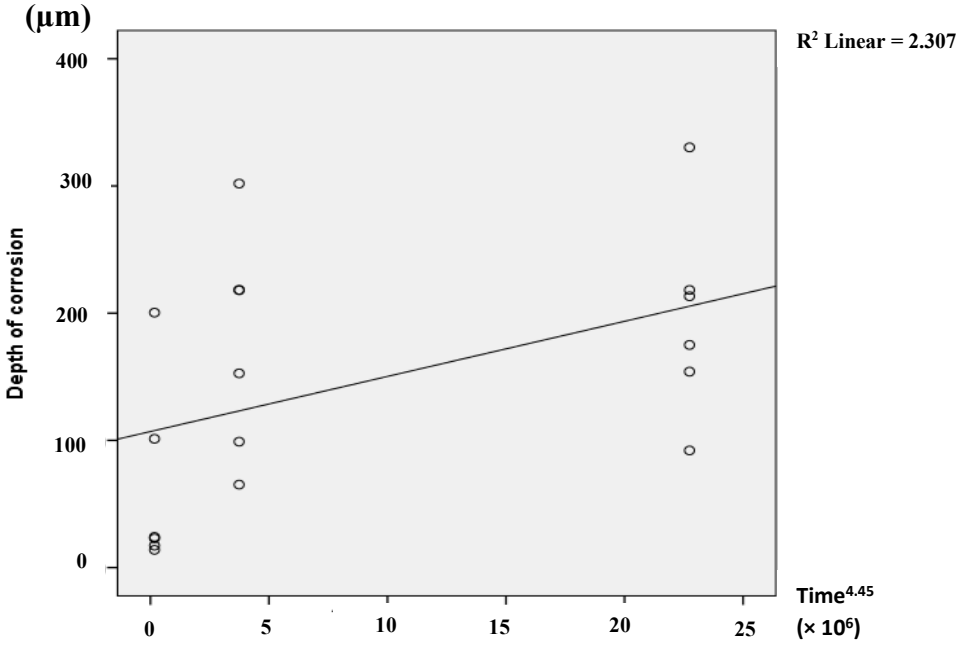

Figure 4.3: Scatter plot of depth of sulfide stress corrosion Vs $Time^{4.45}$ load

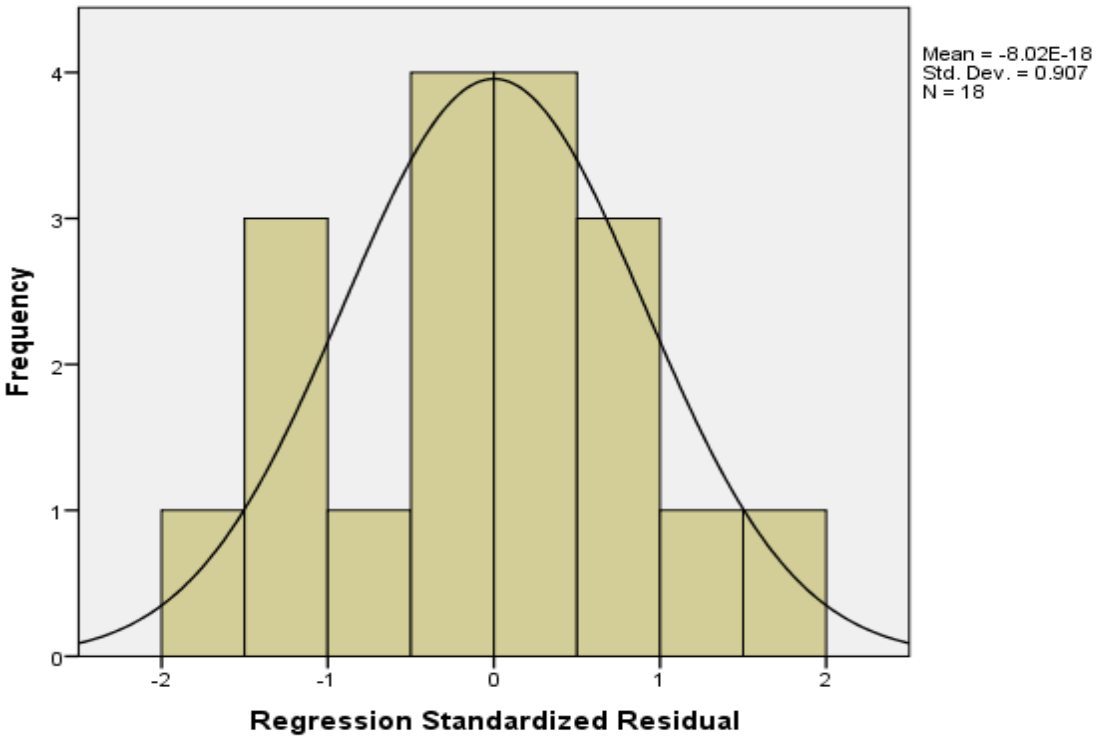

Figure 4.4: Histogram of frequency Vs Regression standardized residual

Table 4.2 shows the Pearson's bivariate correlation matrix for the dependent variables and independent variables.

Table 4. 2: Pearson's correlation matrix

Variable	Depth of sulfide stress Corrosion	e^{pH}	$Time^{4.45}$	1/Load
Depth of sulfide stress corrosion	1.000	-0.487	0.455	-0.526
e^{pH}	-0.487	1.000	0.000	0.000
$Time^{4.45}$	0.455	0.000	1.000	0.000
1/load	-0.526	0.000	0.000	1.000

It can be seen that all correlation coefficients are less than 0.08 other than the coefficient between time$^{0.455}$ and depth of sulfide stress corrosion. Therefore it can be considered that the multicollinearity in data is negligible.

Variance inflation factor (VIF), Tolerance and condition index were tested for the multicollinearity diagnostics and tolerance values (Table 4.3) for all dimensions are 1 (>>>0.1). It proves again that the multicollinearity in data is negligible.

Furthermore, VIF values and condition index values that were obtained for model dimensions indicate that they are less than 10 (Table 4.3). Therefore these values evident that no multicollinearity found in the data.

Table 4.3: Collinearity diagnostic tables

Model dimensions	Tolerance	VIF	Condition Index
Constant	1.000	1.000	1.000
e^{pH}	1.000	1.000	2.661
1/Applied Load	1.000	1.000	5.690
Time$^{4.45}$	1.000	1.000	10.353

The autocorrelation was tested by Durbin Watson test and statistic says the value is 1.343. This indicates that the residuals are not linearly auto correlated. Hence autocorrelation in data is negligible.

The homoscedasticity of data was tested using scatter plots of standardized residuals vs standardized predicted values (Figure 4.4) and standardized residuals vs unstandardized predicated values (Figure 4.5). Both the scatter plots are rectangular enough to conclude the homoscedasticity in data.

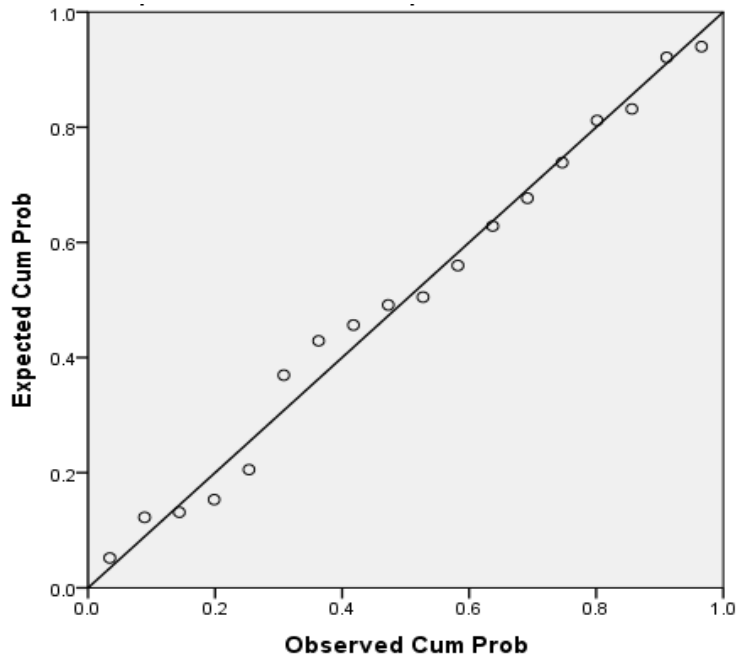

Figure 4.5: Normal P-P plot of regression standardized residuals

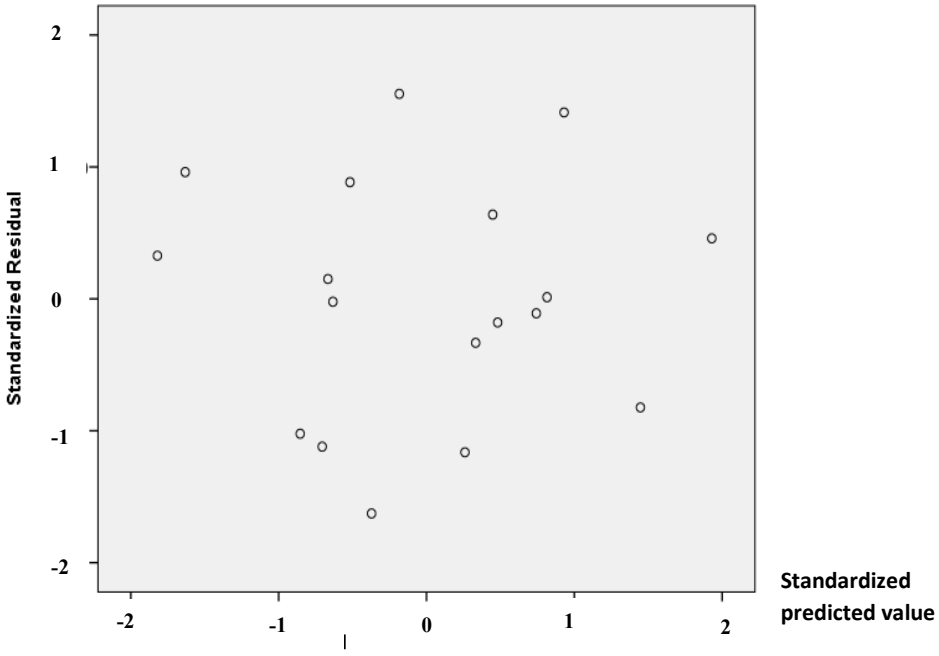

Figure 4. 6: Scatter plot of standardized residuals Vs standardized predicted values

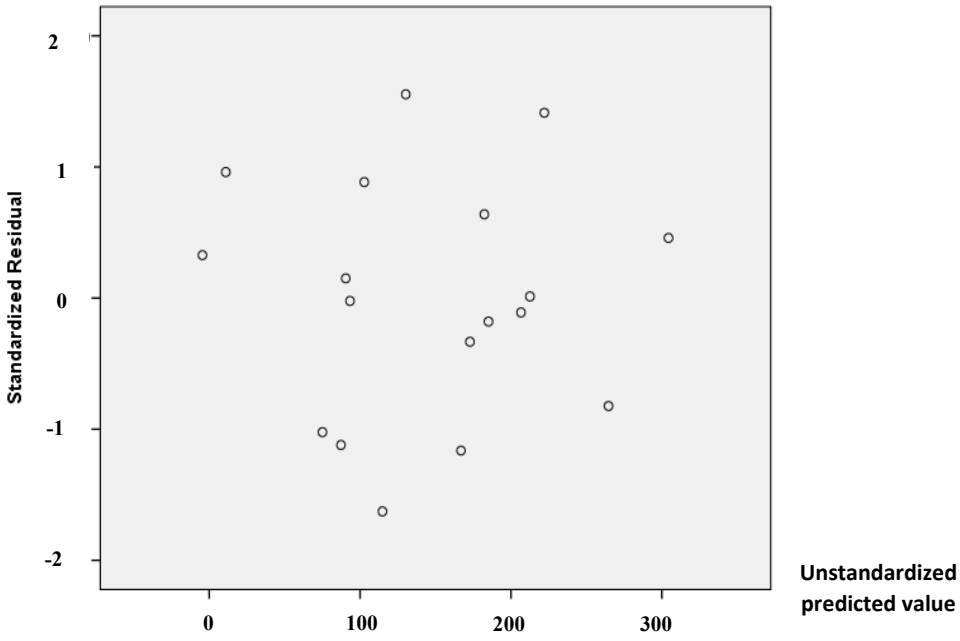

Figure 4.7: Scatter plot of standardized residuals Vs unstandardized predicted values

4.2 Validation of the Model

4.2.1 Validation of the model based on the predetermined test environmental conditions

Model predictions were compared with the experimental values that were used to develop the model as shown in Figure 4.8. Table 4.4 illustrates the test environmental conditions that are given by numbers in Figure 4.8. The range of parameters considered are such that pH values vary between 2.7 and 3.7, applied loads vary among 400N, 600N, 800N and time durations vary among 15 days, 30 days and 45 days.

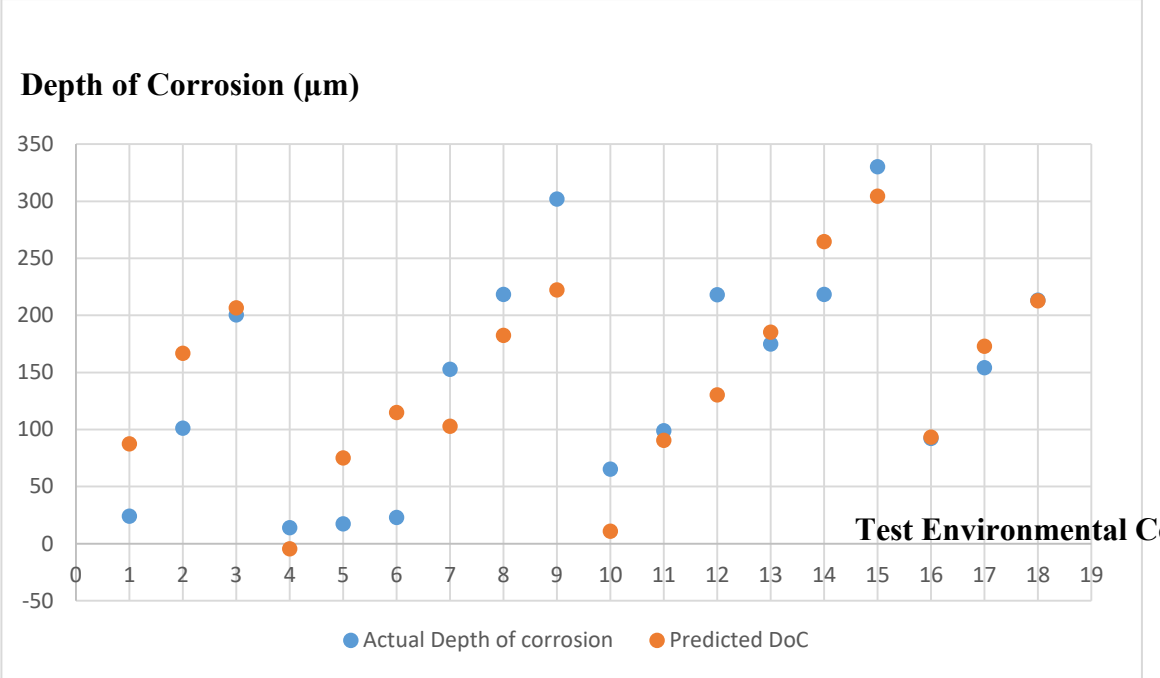

Figure 4.8: The comparison of model predicted values and experimental values of depth of sulfide stress corrosion at 27 ^{0}C and 1 atm under different test environmental conditions

Table 4.4 : Test environmental conditions given by specific numbers in Figure 4.8 and corresponding depths of corrosion.

Test environmental condition	pH Value	Applied Load (N)	Time (Days)	Experiment depth of corrosion(µm)
1	2.7	400	15	24.06
2	2.7	600	15	101.23
3	2.7	800	15	200.45
4	3.5	400	15	13.97
5	3.5	600	15	17.32
6	3.5	800	15	22.97
7	2.7	400	30	152.70
8	2.7	600	30	218.40
9	2.7	800	30	301.90
10	3.5	400	30	65.20
11	3.5	600	30	99.00

12	3.5	800	30	218.00
13	2.7	400	45	175.00
14	2.7	600	45	218.20
15	2.7	800	45	330.30
16	3.5	400	45	92.05
17	3.5	600	45	154.00
18	3.5	800	45	213.30

It can be seen in Figure 4.8 that the depth of sulfide stress corrosion is varying with the test environmental condition similar to the behavior of a wave. The variation of experimental values of depth of corrosion under different test environment is well agreed with the model prediction values. It can be seen that the model successfully captures the upward and downward trends of depth of sulfide stress corrosion with time duration, applied load and pH value. From test environmental condition 1 to 3, there can be seen an increment of depth of corrosion. But the test environmental condition 4 illustrates a sudden reduction of depth of sulfide stress corrosion. Again, it is seen an increment of depth of sulfide stress corrosion from test condition 4 to 6. If we identify one set of depths of corrosion values which are monotonically increased, as a one cluster, it can be seen three clusters up to the test environmental condition 10. Every cluster includes three depth of corrosion values under the applied loads of 400N, 600N and 800N each. But the pH values and the time durations did not follow any fixed pattern or a fixed value within a certain cluster.

This behavior is disobeyed from 10^{th} test environmental condition onwards. According to the previous pattern, test environmental condition 13 should have a less depth of corrosion value compared to the depth of corrosion value shown at test environmental condition 12. Instead, the depth of corrosion values are monotonically increased from test environmental condition 10 to 15. However, the reduction of depth of corrosion at the 13^{th} environmental condition was observed in the experimental depth of corrosions. The test environmental condition 10 to 15 differ from test environmental condition 1 to 10 mainly by time duration. The usual cluster pattern behavior starts to be disobeyed at 13^{th} environmental condition when the time duration gets 45 days. The cluster pattern

behavior occurred from 15th test environmental condition onwards cannot be predicted properly as experiments were continued only up to 18 test environmental condition.

4.2.2 Validation of the model based on the random test environmental conditions.

Model predictions were further compared with experimental results obtained at random test environmental conditions. The test environmental conditions were maintained within the two extremes of pH = 3.7, Applied load = 400N, Time duration = 15 days and pH value = 2.7, Applied load = 800N, Time duration = 45 days. Figure 4.9 shows the comparison between model prediction values and the experimental results obtained at random test environmental conditions. Table 4.5 shows the corresponding test environmental condition maintained at the temperature of 27 ^{0}C and the pressure of 1 atm. It can be seen that the trend line of predicted depth of corrosion values keep a reasonable agreement with the trend line of experimental depth of corrosion values.

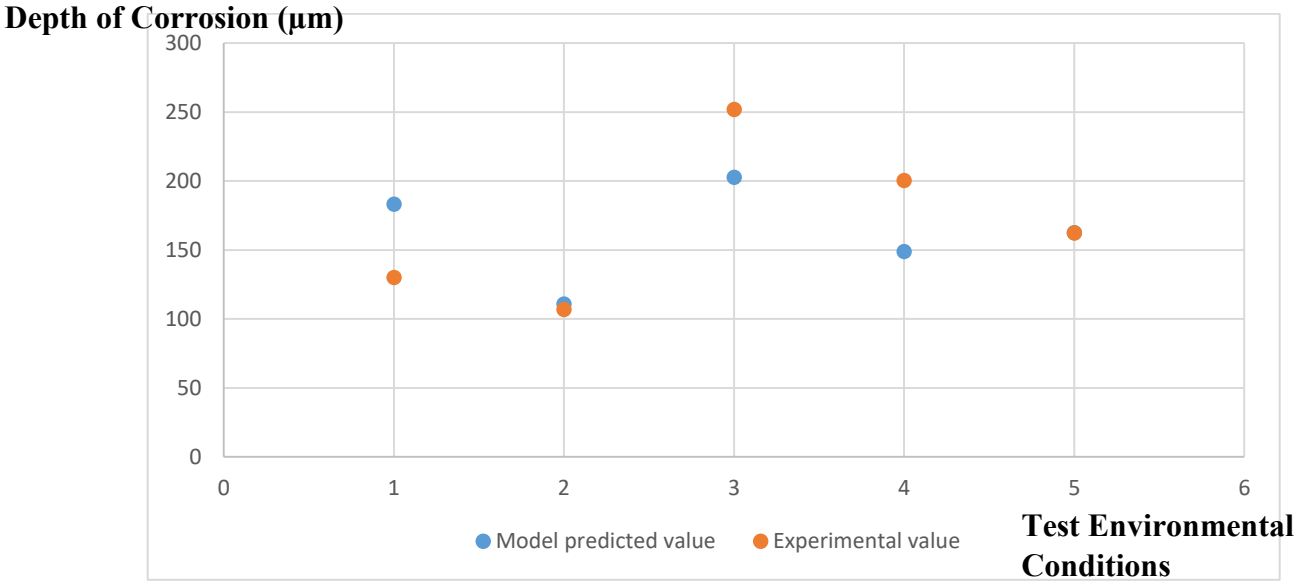

Figure 4.9: comparison between model prediction values and the experimental results

Table 4.5: Test environmental conditions given by numbers in Figure 4.9

No	pH	Applied load	Time
1	2.9	750	18
2	3	500	20
3	2.8	700	32
4	3.3	650	38
5	3.5	550	42

4.3 Limitations of the model

Although the model predicted values follow the upward and downward trends of experimental trend lines (Figure 4.8 and Figure 4.9), it can be seen that the model is predicting lower depth of corrosion values at some of the test environmental conditions, especially when the time duration closes to 30 days. Figure 4.8 shows that all the predicted depth of corrosion values from test environmental condition 7 to 12 are less compared to the experimental depth of corrosion values. The similar trend is observed in Figure 4.9 as well.

The model encounter only the transverse depth of corrosion through the cross sectional area. It doesn't encounter the lateral growth of SSC cracks. However the transverse growth is the dominant growth behavior that can be seen in most of the test environmental conditions.

The minimum depth of corrosion value which was detected at the test environmental condition number 4 mentioned in table 4.4 has the pH value of 3.7, applied load of 400N and time duration of 15 days. But this test environmental condition gives a minus value for predicted depth of sulfide stress corrosion. However, the model starts showing a positive value for the depth of corrosion when applied load gets 408 N or higher values when pH value is 3.7 and time duration is 15 days. Therefore the model gives acceptable

positive depth of corrosion values if the test environmental conditions are maintained under the following parameter ranges shown in table 4.6.

Table 4. 6: Parameter ranges defined for the model at temperature 27 ^{0}C and the pressure 1 atm.

Parameter	Minimum value	Maximum value
Applied load	408 N	800 N
pH value	2.7	3.5
Time duration	15 days	30 days

4.4 Interpretation of behavior of SSC by SEM/EDAX analysis

Experimental results indicated that the time period is the controlling factor in initiation of cracks. Figure 4.10 shows the SEM image of cross section of the steel sample which is not indicating the crack initiating on the 14th day under test condition of pH value 3.5 and applied load 600. According to Figure 4.11, it is obvious that crack was initiated after 15 days under the same condition. Therefore at the primary stage, based on the experimental results, it was concluded that initiation of cracks under all aforementioned 18 conditions occurs after an incubation period of 15 days irrespective of the pH value and applied load.

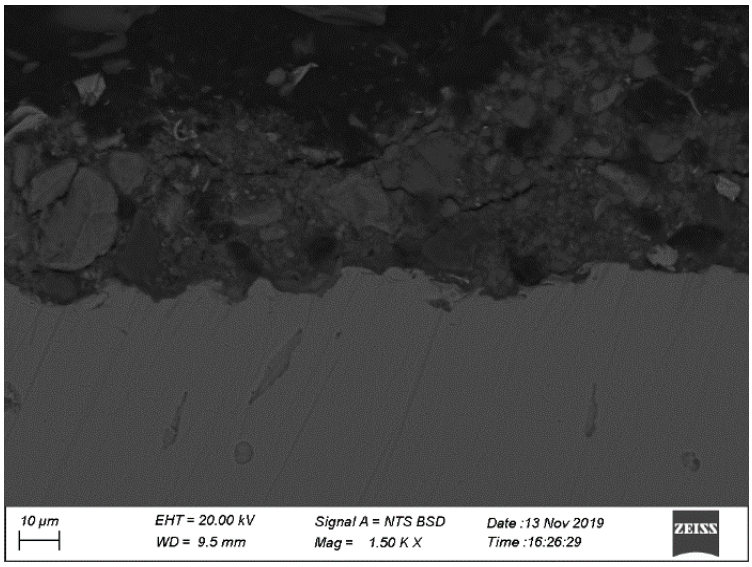

Figure 4.10: SEM image of the cross section of a specimen under the test conditions of pH value – 3.5, Load – 600 N, Time duration - 14 days

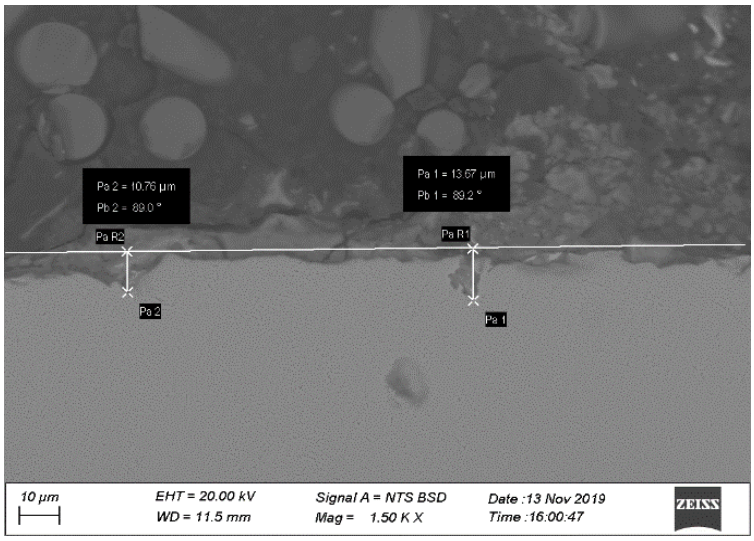

Figure 4.11: SEM image of the cross section of a specimen under the test conditions of pH value = 3.5, applied load = 600 N and time duration = 15 days

The initiation and propagation of sulfide stress cracks were investigated by SEM/EDAX analysis. The sulfur distribution along the crack was observed by SEM/EDAX elemental line profile as shown in Figure 4.12 which clearly shows the higher content of sulfur associated with the crack relative to the other portions of the base metal. Therefore, these cracks can be identified as sulfide stress cracks.

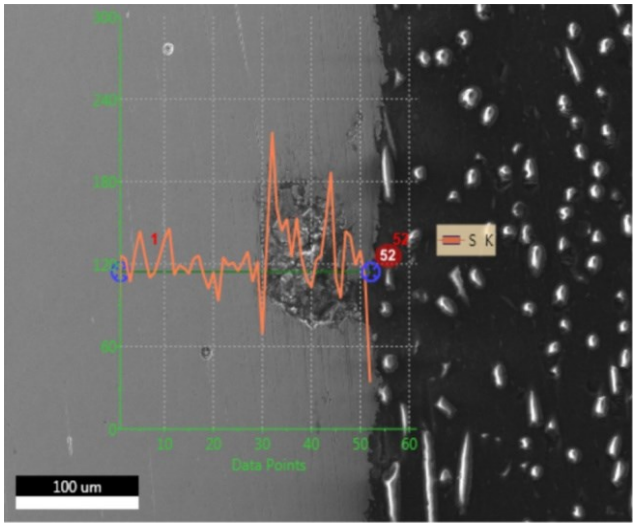

Figure 4.12: Elemental profile plot of the cross section of a specimen under the test conditions of pH value – 2.7, Load – 600 N, Time duration –15 days

The initiation of a sulfide stress crack occur if there are surface discontinuities or surface pits [28]. The formation of pits is a result of ruptures in the surface of Mackinawite layers where the Mackinawite is the predominant iron sulfide polymorph present in corrosion product in the sour environment. Once the Mackinawite layers get a certain thickness, they are ruptured leading to the formation of pits. These pits get filled with Mackinawite with the time [4]. Later these pits are grown to cracks [4].

Once the initiation occurs, the crack starts to propagate transversely inwards to the core of the steel. The crack is penetrated to the steel making branches similar to a growth of a taproot as shown in Figure 4.13.

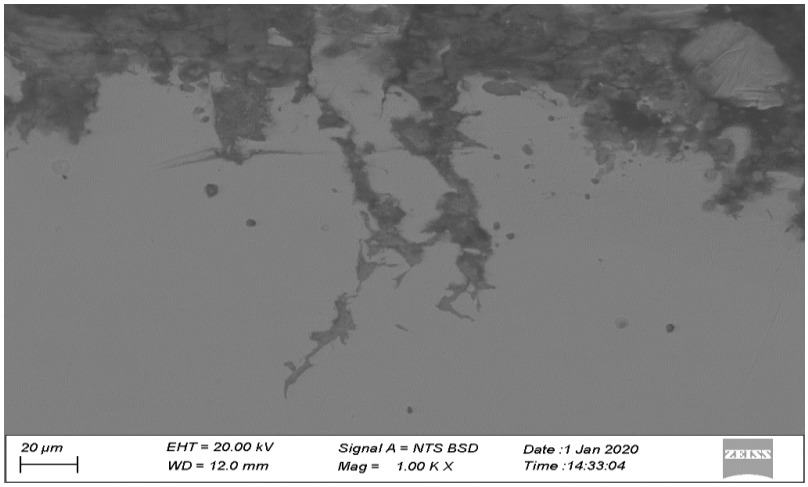

Figure 4.13: SEM image of the cross section of a specimen under the test conditions of pH value = 2.7, applied load = 400 N and time duration = 30

SEM-EDAX elemental line profiles obtained for corroded samples in 30 days showed an interesting behavior in the distribution of sulfur content throughout the crack. A sulfur enriched area which was closer to the middle of the crack length was observed (Figure 4.14).

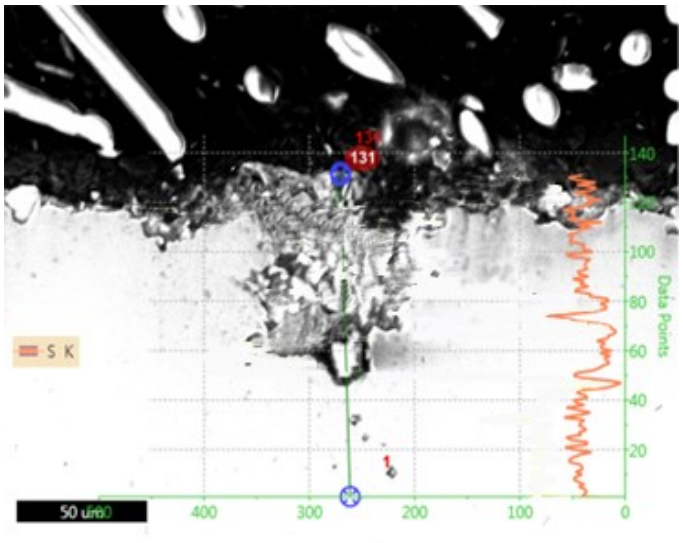

Figure 4.14: Elemental profile plot of the cross section of a specimen under the test conditions of pH value – 3.5, Load – 600 N, Time duration – 30 days

The behavior of formation of sulfur enriched area specifically closer to the middle of the crack length relative to the crack initiation and tip areas can be described based on the mechanism of the propagation of sulfide stress cracks.

The propagation of sulfide stress cracks is associated with the formation of Mackinawite which is the predominant iron sulfide polymorph present in corrosion products in the sour environment. The corrosion product is rich with polymorphs of FeS and $FeCO_3$.

In the sour environment, at high H_2S concentrations, Mackinawite is the predominant component over iron carbonate in the corrosion layer, at low H_2S concentrations, both iron carbonate and Mackinawite may presence in the corrosion product [47]. Under both of the conditions, Mackinawite forms very rapidly on the surface as a very thin, tightly adherent film [4]. Mackinawite is formed through the direct heterogeneous reactions between S^{2-} and Fe^{2+}[13] [14] [15].

Once the Mackinawite film is formed, it starts reverse reaction to dissolve the formed Mackinawite layers [4]. If the formation rate of Mackinawite is greater than the dissolution rate, Mackinawite layer begins to grow covering the whole base metal. The continuous formation of Mackinawite layer causes to form multiple ruptures and these ruptures act as pathways that allows the solution access to the Mackinawite – base metal interface for continued corrosion via a tortuous path.

Mackinawite is an electron conductor. The metal surface which is underneath the Mackinawite layer dissolves forming Fe^{2+}. The electrons removed from iron atom are conducted through Mackinawite layer resulting cathodic reduction of hydrogen on the interlayer of Mackinawite and bulk solution.

When the lattice parameter of Mackinawite crystal structure (Figure 2.1) is considered, c dimension of the Mackinawite crystal lattice is much larger than the a –b dimension (5.03 Å vs. 3.67 Å). It forms an almost sheet like structure. [4]

Because of this sheet like structure, Mackinawite can absorb divalent metallic cation into the lattice as shown in Figure 2.2. Rather than substituting the cations for Fe^{2+} in the Mackinawite structure, the adsorbed cations are moved between the “sheets” of iron sulfide [25][48]. Therefore Fe^{2+} ions which are formed at the anodic sites on the metal

surface should be able to migrate away from the metal surface towards the film-electrolyte boundary by moving along this path. Fe^{2+} ions which are formed on the metal surface can find film electrolyte along the ruptured pathways and within the interlayer of Mackinawite - bulk solution. The Fe^{2+} ions which are diffusing out through the ruptured pathway can form FeS only along these ruptured pathways and the Fe^{2+} ions which are moving along the planes of the Mackinawite can form FeS once it meets a sudden ruptured pathway or once it meets the interlayer of bulk solution and top surface of the Mackinawite.

When a cross section of a crack is selected, very less Mackinawite should be formed closer to the crack tip and more Mackinawite should be formed closer to the crack initiation point. Therefore it can be expected that the ruptures along the crack length should be increased from crack initiation to crack tip. Similarly the pathways for solution to enter to the crack should be increased from crack initiation to crack tip.

Therefore, when Fe^{2+} ions move upwards along the Mackinawite sheets, there is a higher possibility to meet more pathways of solution closer to the middle of the crack. Once they meet solution pathways, FeS is formed through direct heterogeneous reactions. Hence, FeS rich area can be seen closer to the middle of the crack (Figure 4.14).

However, the microstructural observations of corroded specimens at 45 days were completely different compared to the observations carried out at 30 days. It was seen that widely spread corrosion cracks instead of branched cracks. Figure 4.15 and Figure 4.16 show microstructures of cross sections of 45 days corroded specimen. In these microstructures, it can clearly be seen a lateral growth of cracks. But the propagation of cracks were transverse across a cross section of a selected specimen up to 30 days.

In addition to that, a selected sulfide stress crack looked like a tap root up to 30 days but a propagated crack looked like a fibrous root at 45 days. The reason for this behavior can easily be explained using the mechanism of hydrogen embrittlement. The main factors of hydrogen embrittlement in metal are metal microstructure, stress intensity and concentration of hydrogen [8]. It is obvious that mild steels are susceptible for hydrogen embrittlement when they are affected by enough stress intensity and hydrogen

concentration. The 30 days microstructures provide enough evidences to state that the cracks were getting enriched with hydrogen during that period.

The elemental profile plots obtained for 30 days corroded specimen indicate that there is a certain location where the FeS concentration gets high (Figure 4.14). FeS is a good hydrogen trapping site. Some of the researches demonstrate that the FeS can act as a reservoir of hydrogen that provides ideal conditions for generating and sustaining hydrogen absorption [49][50].

Since the Mackinawite filled cracks provide pathways for bulk solution to move through the crack, FeS rich areas can easily be enriched with H ions and H atoms as bulk solution is rich with H^+. Therefore it can be considered that the specific locations that get rich with FeS get rich with Hydrogen as well.

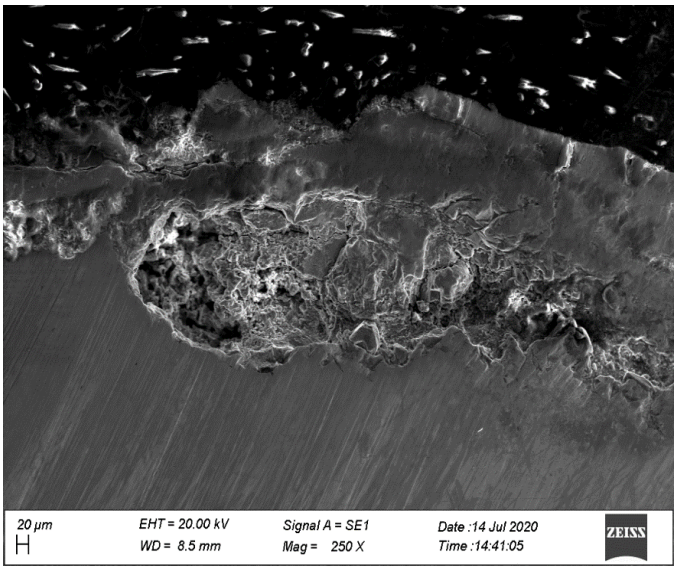

Figure 4.15: SEM image of the cross section of a specimen under the test conditions of pH value – 2.7, Load – 800 N, Time duration – 45 days

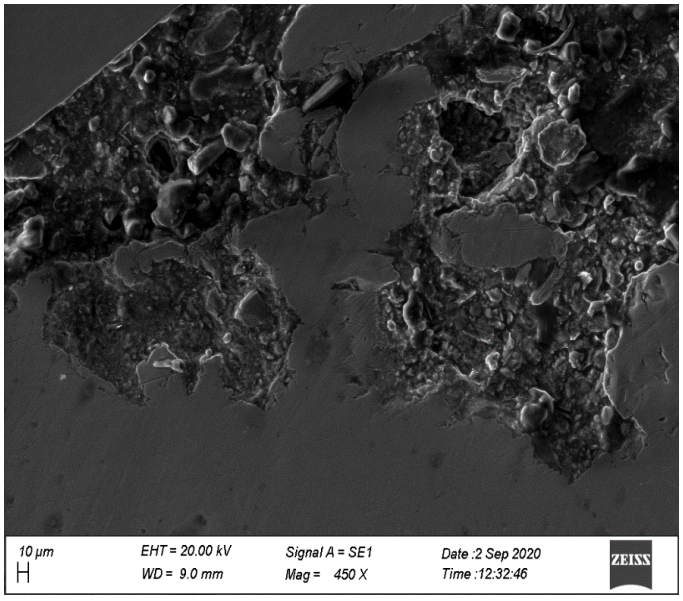

Figure 4.16: SEM image of the cross section of a specimen under the test conditions of pH value – 3.5, Load – 800 N, Time duration – 45 days

These enrichment of H provide ideal environment for hydrogen embrittlement. As it mentions in the literature survey, there are four types of mechanism that hydrogen embrittlement can occur. They are known as hydrogen pressure theory, hydrogen enhanced decohesion, hydrogen enhanced localized plasticity and stress induced hydride formation.

Out of these four mechanisms, hydrogen enhanced decohesion and hydrogen enhanced localized plasticity theories can be used to explain the lateral growth of the crack.

According to hydrogen enhanced decohesion, trapped hydrogen may diffuse into rain boundaries, interstitials and precipitates weakening the interatomic bonding under stress leading to cracks. As the top and bottom areas of sulfur enriched areas are filled with Mackinawite, diffusion of trapped H should happen laterally causing the lateral growth of cracks. Further decohesion theory states that the crack tips and the crack vicinity are subjected to maximum tensile stresses when the hydrogen are trapped within a crack. The periphery of the crack in the region where FeS content is high can act as a crack tip. Hence the periphery of the crack should enhance lateral growth.

According to hydrogen enhanced localized plasticity theory, hydrogen concentration at the hydrogen rich area causes deformation at the periphery of the crack. These deformations increases plasticity of the metal. Further hydrogen diffuse at dislocation core increasing dramatically the internal stresses. These stresses make cracks around the periphery of the crack. It causes for the lateral growth of cracks.

5 CONCLUSIONS

The depth of sulfide stress corrosion of API 5L Grade B corresponding to the specific combination of pH value (2.7 – 3.5), applied load/pressure (400N – 800N) and time duration (15 to 45 days) under ambient temperature and atmospheric pressure can be predicted using the developed model. Out of these three factors/variables, it can be concluded that the time duration is the leading factor that causes crack initiation and propagation of sulfide stress corrosion. Although the developed model successfully follows the experimental results, it underestimates the depth of sulfide stress corrosion when the time duration gets values closer to 30 days.

The propagation behavior of sulfide stress corrosion can clearly be explained using SEM-EDAX elemental line profiles obtained for different directions of the propagated cracks. The observation of formation of sulfur enriched area which was closer to the middle of the crack length can be explained by relating the downward movement of H_2S solution along the raptured pathways formed in the cracks and upward movement of Fe^{2+} ions along the Mackinawite sheets. Hence it can be concluded that the Mackinawite formed as a corrosion product plays a dominant role in the propagation of sulfide stress corrosion. The lateral growth had been begun in between 30 to 45 days. The trapped hydrogen associated with the higher FeS content in the region closer to the middle of the crack length is the dominant factor leading to the lateral growth of cracks.

The propagation of the lateral growth observed in this work could be explained based on the hydrogen enhanced de-cohesion theory and hydrogen enhanced localized plasticity theory.

6 RECOMMENDATIONS

The developed model can predict the depth of sulfide stress corrosion only up to 45 days of time duration. Therefore, the prediction of depth of corrosion under the time durations which are beyond 45 days may be inaccurate. Hence, it is recommended to expand the time duration which is considered for the development of the model till the failure of the test specimen.

As section 4.3 addresses, the model doesn't encounter the lateral growth of SSC which occurred in between 30 to 45 days. Therefore, the model can be further developed to predict the lateral growth of SSC cracks.

7 REFERENCES

[1] W. Sun, Dylan, V. Pugh, Stephen, N. Smith, S Ling, L. Jorge., Pacheco,J. Robert, and Franco, "A Parametric Study of Sour Corrosion of Carbon Steel," *Acta Metallurgica,* vol. 44, no. 2, pp. 20, 1996.

[2] S. N. Smith, and M. Joosten, "Corrosion of carbon steel by H_2S in CO_2 containing oilfield environments," presented at the NACE International, Houstan, Texas, 2006.

[3] H. Asahi, M. Ueno, and T. Yonezawa, "Prediction of sulfide stress cracking in high-strength tubulars," *Corrosion,* vol. 50, no. 7, pp. 537-545, 1994.

[4] Smith, and N. Stephen, "Current understanding of corrosion mechanisms due to H_2S in oil and gas production environments," presented at the NACE - International Corrosion Conference Series, Houstan, Texas, 2015.

[5] I. H. Omar, Y. M. Gunaltun, J. Kvarekval, and A. Dugstad, "H_2S corrosion of carbon steel under simulated Kashagan field conditions," presented at the NACE international, Houstan, Texas, 2005.

[6] W. Sun, S. Nesic, and S. Papavinasam, "Kinetics of corrosion layer formation,Part 2 – iron sulfide and mixed iron sulfide / carbonate layers," *Corrosion,* vol. 7, no. 64, pp. 586-599, 2008.

[7] J. Gossett, "Detecting sulfide stress cracking and applying NACE MR0175," *Chemical week,* August 2000, 2018.

[8] R. Garber, T. Wada, E B. Fletcher, and T. B. Cox, "Sulfide stress cracking resistant steels for heavy section wellhead components.," *Materials For Energy systems,* vol. 7, no. 2, pp. 338 - 350, 1987.

[9] Wood, M. Heraty,V. Arellano, A. Lisa,V. Wijk, and Lorenzo, Corrosion - related accidents in petroleum refineries, Italy: European commission joint research centre institute for the protection and security of the citizen, 2013.

[10] Octal Online (2012). Available: https://www.octalsteel.com/resources/api-5l-grade-b-pipe. [Accessed 2021].

[11] Y. P. Asmara, A. Juliawati, A.Sulaiman and Jamiluddin, "Mechanistic model of stress corrosion cracking (scc) of carbon steel in acidic solution with presence of H_2S," presented at the International Conference on Mechanical Engineering Research (ICMER2013), Bukit gambang resort city, Kuantan, Pahang, Malaysia,

2013.

[12] W. Sun and S. Nesic, "A mechanistic model of H_2S corrosion of mild steel," presented at the corrosion 2007 conference & Expo, Athens, Ohio, 2007.

[13] Y. Zheng, J. Ning, B. Brown and S. Nesic, "Electrochemical model of mild steel corrosion in a mixed H_2S/CO_2 aqueous environment," *Corrosion,* no. 3907, pp. 1-20, 2014.

[14] S. N. Smith, "Predicting corrsosion in slighlty sour environment," *Materials performance,* 2002

[15] K. Liao, Q. Yao, X. Wu, and W. Jia , "A numerical corrosion rate prediction method for direct assessment of wet gas gathering pipelines internal corrosion," *Energies,* vol. 5, no. 10, pp. 3892-3907, 2012.

[16] A. Traidia, E. Chatzidouros, and M. Jouiad, "Review of hydrogen-assisted cracking models for application to service lifetime prediction and challenges in the oil and gas industry," *Corrosion,* vol. 36, no. 4, pp. 323-347, 2018.

[17] C. Zapffe, and C. Sims, "Hydrogen embrittlement, internal stress and defects in steel.," *Trans AIME 1941,* vol. 1307, pp. 1-37, 1941.

[18] H.K. Birnbaum, and P. Sofronis, "Hydrogen-enhanced localized plasticity – a mechanism for hydrogen-related fracture," *Material Science and Engineering,* vol. 176, pp. 191-202, 1994.

[19] R.A. Oriani, " A mechanistic theory of hydrogen embrittlement of steels," *Berichte Der Bunsengesellschaft Für Phys Chem,* vol. 76, pp. 848-857, 1972.

[20] H. K. Birnbaum and P. Sofronis, "Hydrogen-enhanced localized plasticity--a mechanism for hydrogen- related fracture," *Materials Science and Engineering,* vol. 176, no. 1-2, pp. 191-202, 1994.

[21] G. Keith , "Electrochemical investigation and modeling of carbon dioxide corrosion of carbon steel in the presence of acetic acid," presented at the NACE International conference, vol. 4379, 2004.

[22] Rickard, David, A. Griffith, A. Oldroyd, I.B. Butler, E. Lopez-Capel, and D.A.C, Manning. “The composition of nanoparticulate mackinawite, tetragonal iron(II) monosulfide”, *Chemical Geology*, Vol. 235, pp 286-298, 2006.

[23] A.J. Devey, R. Grau-Crespo and N. H. de Leeuw, "Combined density functional

theory and interatomic potential study of the bulk and surface structures and properties of the iron sulfide mackinawite (FeS)," *J Phys. Chem,* vol. 112, pp. 10960-10967, 2008.

[24] Pearce, Carolyn, Richard, A.D. Patrick and D. J. Vaughan, "Electrical and magnetic properties of sulfides," *Reviews in Mineralogy and Geochemistry,* vol. 61, pp. 127-180, 2006.

[25] Zhao, J.M, Z. Wei, Y. Zuo and X.H. Zhao, "Effects of some ions on ion-selectivity of ferrous sulfide," *Journal of Applied Electrochemistry,* vol. 35, pp. 267-271, 2005.

[26] B. Brown, D. Young, and S. Nesic, "Localized Corrosion in an H_2S/CO_2 Environment," in *17th International Corrosion Conference*, 2008.

[27] B. Brown, and S. Nesic, "Aspects of Localized Corrosion in an H_2S / CO_2 Environment," in corrosion 2012, 2012.

[28] S.M.R. Ziaei , A. H. Kokabi, and M. Nasr-Esfehani, "Sulfide stress corrosion cracking and hydrogen induced cracking of A216-WCC wellhead flow control valve body," *Case Studies in Engineering Failure Analysis,* vol. 1, no. 3, pp. 223-234, 2013.

[29] M. Liu, C.D.Yang, G.H. Cao, A. M. Russell and Y.H. Liu, "Effect of microstructure and crystallography on sulfide stress cracking in API-5CT-C110 casing steel," *Materials Science and Engineering ,* vol. 671, pp. 244-253, 2016.

[30] A. Turnbull, D.H. Ferriss and H. Anzai, "Modelling of the hydrogen distribution at a crack tip," *Materials Science and Engineering,* vol. 206, no. 1, pp. 1-13, 1996.

[31] K. N. Akhurst and T. J. Baker, "The threshold stress intensity for hydrogen-induced crack growth," *Physical metallurgy and materials science,* vol. 12 A, no. 6, pp. 1059-1070, 1981.

[32] H. Huang and W. W. Gerberic, "Quasi-equilibrium modeling of the toughness transition during semibrittle cleavage," *Acta metall,* vol. 42, no. 3, pp. 639-647, 1994.

[33] S. Serebrinsky, E. Carter, and M. Ortiz, "A quantum-mechanically informed continuum model of hydrogen embrittlement," *Journal of the Mechanics and Physics of Solids,* vol. 52, no. 10, pp. 2403-2430, 2004.

[34] K. Lee, Laboratory Notebook of Institute for Corrosion and Multiphase techonology, ohio: Ohio University, 2005.

[35] Y. Choi, S. Nesic, and S. Ling, "Effect of H2S on the CO2 Corrosion of Carbon Steel in Acidic Solutions," *Electrochim. Acta 56,* vol. 4, pp. 1752-1760, 2011.

[36] J. Jeon, "Sulfide stress cracking behavior of grade c-110, q-125 and t-95 steel tubulars under high-pressure conditions," *jiwon jeon*, Oklohoma, 2016.

[37] R. Morana and P.I. Nice, "Corrosion assessment of high strength carbon steel grades P-110, Q-125, 140 and 150 for H_2S containing well environments," presented at the corrosion 2009, nace international, Atlanta, Georgia, 2009.

[38] J.C. Maria, and T. Perez, "Ibp3507_10 sulfide stress cracking susceptibility of high strength steels used in oil and gas industry: the effect of environmental and microstructural factors," presented at the Rio Oil & Gas Expo and Conference 2010, Rio de Janeiro, 2010.

[39] M. Zhaoa, M. Liu, A. Atrens, Y. Shan, K. Yang, "Effect of applied stress and microstructure on sulfide stress cracking resistance of pipeline steels subject to hydrogen sulfid," *Materials Science and Engineering ,* vol. 478, no. 1-2, pp. 43-47, 2008.

[40] J. P. Hirth, "Effects of Hydrogen on the Properties of Iron and Steel," *Metallurgical Transactions ,* vol. 11, no. 6, pp. 861-890, 1980.

[41] Q. Aviles, J. Marlene, H. Ladino, Duberney, Falleiros, N. Alonso de melo, and H. Gomes, "A comparative investigation of the corrosion resistance and HiC suceptibility of API 5L X65 and API 5L X80 steels," *Materials Research,* vol. 22, no. 1, pp. 1-13, 2019.

[42] M. D. Tumuluru, "Sulfide Stress Corrosion Cracking in Low-Alloy Steel Inertia Friction Welds.," *Welding Journal (Miami, Fla),* vol. 66, no. 3, 1987.

[43] *Standard test method laboratory testing of metals for resistance to sulfide stress cracking and stress corrosion cracking in H_2S environments*, ANSI/NACE TM0177-2016.

[44] *Pipeline Transportation Systems for Liquids and Slurries,* ASME B31.4*,* The american society of mechanical engineers, Washington, 2012.

[45] "Pipeline Basics & Specifics About Natural Gas Pipelines," pipeline safety trust ,

Bellingham, washington,USA, 2015.

[46] StatisticsSolutions online (2016) Available: http://www.statisticssolutions.com. [Accessed 2021].

[47] W. Sun and S Nesic, "Kinetics of Corrosion Layer Formation . Part 2 — Iron Sulfi de and Mixed Iron Sulfi de / Carbonate Layers in Carbon Dioxide / Hydrogen Sulfi de Corrosion," *Corrosion,* july, pp. 586-589, 2008.

[48] Liu, Jianrong, T. Kalliat, Valsaraj, I. Devai and R.D. Delaune, "Immobilization of aqueous," *Journal of Hazardous Materials ,* vol. 157, p. 432–440, 2008.

[49] Wallaert, Elien, Depover, Tom, Graeve, Iris, Verbeken, and Kim, "FeS corrosion products formation and hydrogen uptake in a sour environment for quenched & tempered steel," *Metals,* vol. 8, no. 1, 2018.

[50] Specification for Line Pipe, American Petroleum Institute, USA, 2000.